

**Entanglement dynamics of many-body quantum states:  
sensitivity to system conditions and a hidden universality**

Devanshu Shekhar and Pragya Shukla

*Department of Physics, Indian Institute of Technology,*

*Kharagpur-721302, West Bengal, India*

(Dated: February 24, 2026)

arXiv:2602.19280v1 [quant-ph] 22 Feb 2026

# Abstract

We consider physical Hamiltonians that can be represented by the multiparametric Gaussian ensembles, theoretically derive the state ensembles for its eigenstates and analyze the effect of varying system conditions on its bipartite entanglement entropy. Our approach leads to a single parametric based common mathematical formulation for the evolution of the entanglement statistics of different states of a given Hamiltonian or different Hamiltonians subjected to same symmetry constraints. The parameter turns out to be a single functional of the system parameters and thereby reveals a deep web of connection hidden underneath different quantum states.

## I. INTRODUCTION

An important requirement of quantum information processing is that any knowledge of the many-body state provides minimum information about its subunits. One way to ensure this is by maximizing the amount of entanglement among the subunits; this in turn leads to an extensive search for the states with maximum entanglement, e.g., an ergodic state (i.e. one accessing all parts of Hilbert space with equal probability). An arbitrary many-body state is however usually non-ergodic with partial entanglement (lying between separability and maximum entanglement). The question is (i) how to quantify its entanglement? (ii) what type of variation of system conditions can lead to an enhancement of entanglement? (iii) whether its entanglement can be preserved in time or under changing system conditions once it reaches the maximum entanglement limit? Notwithstanding intense research efforts in past two decades, the answers to many such questions are still not available. The growth of entanglement among subunits with time also renders the analysis beyond the access of numerical techniques. This motivates us to seek new theoretical routes to investigate many-body entanglement and thereby gain insights in the non-equilibrium quantum dynamics.

In general, the interactions among various subunits of a many-body system are sensitive to a host of system conditions, both static as well dynamic type. A variation of these conditions can lead to changes in the mutual interactions among subunits and is expected to manifest, thereby, in the dynamics of entanglement measures too, more clearly if the dynamics is analyzed in the non-interacting basis, i.e., product states of subunits. Indeed, the ideally sought information in context of many-body systems is the one that describes multi-partite entanglement for a fixed set of system conditions as well its variation with

changing interactions among various parts; the technical complexity however renders the determination a very difficult task. Fortunately many important insights can still be achieved by consideration of the entanglement between its two sub-parts, referred as the bipartite entanglement and is the main objective of the present study.

The standard route to determine the entanglement measures for a pure state requires a prior knowledge of the density matrix  $\rho = |\Psi\rangle\langle\Psi|$ . The latter can in turn be obtained by solving the eigenvalue equation for the Hamiltonian, determining its states and then calculation of the state matrix. An alternative route adopted in many previous studies was either based on direct modelling of the state matrix ensemble, e.g., by a Ginibre ensemble leading to a stationary Wishart ensemble (e.g. [1–6]) or its generalizations, e.g., [7–9]. Although these studies provided many insights, they lacked a very important aspect: as the state matrix ensemble was derived without any reference to underlying Hamiltonian, the connection of ensemble parameters with system parameters was not explicit. This handicaps one from a direct analysis of the entanglement dynamics with changing system parameters. The primary objective of our present study is to fulfil this information gap.

To achieve our objective, we first need to determine the matrix representation of the Hamiltonian in a physically motivated basis and thereafter its eigenstates. A many-body Hamiltonian however consists of complicated interactions among its subunits which even if well-known, e.g., coulomb interactions, an exact determination of its matrix elements is not often possible; this could occur, for example, due to technical issues encountered in calculation of the integrals either by theoretical or numerical route. The incomplete knowledge or error in their determination manifests itself by randomization of the matrix elements. Indeed, the nature and type of the distribution of the matrix elements is sensitive to various system conditions, e.g., symmetry and conservation laws, dimensionality and boundary conditions, disorder etc. and can vary from one element to the other. As a consequence, the Hamiltonian matrix is best represented by a system-dependent random matrix, with some or all elements randomly distributed, the type and the strength of the latter in general sensitive to underlying system conditions.

As expected, based on eigenvalue equation, the randomness underlying the matrix elements manifests in the eigenstates of the Hamiltonian too and the distribution of the latter can be derived, in principle, from the JPDF of the former by a transformation of variables from matrix space to eigenvalue-eigenstate space. An integration of the ensemble density of

the Hamiltonian, i.e, the JPDF of the matrix elements is in general technically complicated, thus motivating a search for alternative routes, e.g., a differential route. As discussed in [10], an evolution equation for the JPDF of the components of an arbitrary eigenstate (referred as state JPDF hereafter for brevity) for a many-body system represented by multiparametric Gaussian ensembles can be derived from the ensemble density. The information can further be used to determine the statistical behavior of the entanglement measures. An additional benefit of the differential route is a common mathematical formulation in terms, of the state JPDF for a wide range of many-body systems where the system information is contained in a single parameter, i.e., the complexity parameter. We pursue the above approach in the present work to derive the evolution equation for the entanglement measures and their solutions.

The paper is organized as follows. We begin, in section II, with two examples of prototypical Hamiltonians: (i) a many-body Hamiltonian modelled by a generalized version of the quantum random energy model (QREM) and (ii) the random-field Heisenberg model (RFHM), their ensemble densities, and the relation between system parameters and ensemble parameters. These examples help to analyze the effect of changing system conditions on the ensemble parameters. Section III describes briefly necessary tools for our approach, i.e, the diffusion equation for the ensemble density of a many-body Hamiltonian in terms of changing ensemble parameters. This is necessary to derive the matrix elements moments used, in section IV, to derive the diffusion equation for the components of an arbitrary many-body state. (An alternative route to derive the equation, based on a direct integration of the Hamiltonian ensemble density, is discussed in [10]). Section V presents the derivation evolution equation of the Schmidt eigenvalues, which is then used in the Section VI in the calculation of the average and variance of an entanglement measure, the von Neumann entropy, for bipartite pure states with varying system conditions. As the theoretical derivations are technically involved, we have moved them to supplementary material [11] to avoid distraction from the significance of our results. Based on the two systems mentioned in section II, we also pursue a numerical verification of our theoretical predictions and find a good agreement; this is described in section VII. We conclude in section VIII with a summary of our ideas, results and open questions.

## II. DEFINITIONS: STATE MATRIX AND ENTANGLEMENT ENTROPIES

Consider a many-body system in a pure state  $|\Psi\rangle$ . The information about the quantum correlations between the two sub-parts is contained in the components of  $|\Psi\rangle$  represented in the bipartite basis, consisting of orthonormal bases of the two sub parts. Assuming the orthogonal subspaces of its sub parts  $A$  and  $B$ , consisting of basis vectors  $|a_k\rangle$  and  $|b_l\rangle$ ,  $k = 1 \rightarrow N_A, l = 1 \rightarrow N_B$  respectively, we can write  $|\Psi\rangle = \sum C_{kl} |a_k\rangle |b_l\rangle$ ; the matrix  $C$  with coefficients  $C_{kl}$  (complex or real) as its entries is referred as the state matrix.

The standard entanglement measures for a pure bipartite state, viz., the von Neumann entropy  $R_1$  and Rényi entropies  $R_n$  with  $n > 1$ , are functions of the eigenvalues of the  $N_A \times N_A$  reduced density matrix  $\rho_A$  for subsystem  $A$  where  $\rho_A = CC^\dagger$ . The eigenvalues of  $\rho_A$  are also referred as the Schmidt eigenvalues. Denoting the latter as  $\lambda_1, \dots, \lambda_N$ , for example, the von Neumann entropy is defined as  $R_1 = -\text{Tr}\rho_A \log\rho_A = -\sum_{n=1}^{N_A} \lambda_n \log\lambda_n$  and  $R_\alpha = \frac{1}{1-\alpha} \ln \text{Tr}(\rho_A)^\alpha = \frac{1}{1-\alpha} \ln \sum_{n=1}^{N_A} \lambda_n^\alpha$ .

## III. HAMILTONIAN AND THE REPRESENTATIVE ENSEMBLE

A determination of the Schmidt eigenvalues requires prior information about the state matrix  $C$ , i.e., the components of  $|\Psi\rangle$  in a bipartite basis. The latter can in principle be obtained by solving the eigenvalue equation  $H|\Psi\rangle = \lambda|\Psi\rangle$  with  $H$ . This in turn requires the determination of the matrix elements of the many-body Hamiltonian in the basis. But, as mentioned in section I, the error associated with exact determination of the matrix elements, further complicated by the fluctuating system conditions, render it necessary to describe the matrix elements by a statistical distribution in a physically motivated basis, e.g., the bipartite basis in the present case. Due to technical complexity of our theoretical ideas, it is helpful to first consider some prototypical examples.

**(i) Quantum random energy model (QREM):** We consider a one dimensional lattice of  $L$  spin 1/2 particles in a random magnetic field, described by the Hamiltonian

$$H = H_{REM} + \Gamma \sum_{i=1}^L \sigma_i^x, \quad (1)$$

where,  $H_{REM} = \sum_k E_k |k\rangle\langle k|$  is the random energy part of the Hamiltonian, diagonal in the  $S_z$  basis  $\{|k\rangle\}$ , such that the energies  $\{E_k\}$  are independent and identically distributed as

$P(E_k; h, L) = \frac{1}{\sqrt{\pi L}} e^{-\frac{E_k^2}{L}}$  and  $\sigma_x$  is one of the Pauli matrices. For  $\Gamma$  as a (negative) constant, eq. (1) corresponds to the Hamiltonian of the well studied QREM [12–15] that can be mapped to an Anderson model on an  $L$ -dimensional hypercube with the spin configurations being lattice sites with a constant hopping strength [13]. For a fixed energy density e.g.  $\epsilon = 0$ , the dynamics of QREM is governed by the transverse-field parameter  $\Gamma$ . In the matrix space, however, this leads to a mere translation of the off-diagonal elements and there is an absence of diffusion. This is the case in general when the variance of all the matrix elements are kept fixed.

For a matrix representation of  $H$ , we choose the product state basis spanned by  $2^L$  vectors of type  $|\mu\rangle \equiv \prod_{k=1}^L |m_k\rangle$  with each  $\sigma_z |m_k\rangle = \pm |m_k\rangle$ . A state  $\Psi$  of  $H$  in this basis can be expressed as  $|\Psi\rangle \equiv \sum_{\mu} \psi_{\mu} |\mu\rangle$ . For the entanglement analysis, we consider a bi-partition of the spin-chain into two equal subparts, referring them as subsystem  $A$  and  $B$  with their local basis spaces as  $|a_{\mu}\rangle$  and  $|b_{\mu}\rangle$ . The basis state  $|\mu\rangle$  can then be written as the  $|\mu\rangle \equiv |a_{\mu} b_{\mu}\rangle$ . The components of  $|\Psi\rangle$  can now be written  $C_{a_{\mu} b_{\mu}}$ :  $\psi_{\mu} \equiv C_{a_{\mu} b_{\mu}} \equiv \langle a_{\mu} b_{\mu} | \Psi \rangle$ . In the  $\sigma_z$  basis, the non-zero off-diagonal elements correspond to the basis states at a Hamming distance one from the diagonal; (this is because  $\sigma_i^x$  flips the spin at only one site  $i$ ). This leads to  $L$  non-zero off-diagonal elements per row in the matrix representation of the Hamiltonian given by eq. (1).

In order to analyze the multiple system parameters dependence for this model, we consider  $\Gamma$  to be a basis-dependent random variable with mean zero and a power-law decaying variance i.e.  $\langle \Gamma_{\mu\nu}^2 \rangle = \frac{1}{1+(\frac{\mu-\nu}{b})^2}$ ,  $\langle \Gamma_{\mu\nu} \rangle = 0$ , which can then be mapped to an Anderson model on an  $L$ -dimensional hypercube with a random and anisotropic hopping strength. This in turn leads to independent Gaussian distributed off-diagonals with mean  $\langle H_{\mu\nu} \rangle = 0$  and variance  $\langle H_{\mu\nu}^2 \rangle = \frac{1}{1+(\frac{f_{\mu\nu}}{b})^2}$  where  $f_{\mu\nu} = |\mu - \nu|^2$  if the basis elements  $\mu$  and  $\nu$  are at a unit Hamming distance from each other,  $f_{\mu\nu} = 0$  otherwise. With diagonal  $H_{kk} = E_k$ , the diagonals  $H_{kk}$  are distributed as Gaussians with zero mean and same variance:  $\rho(H_{\mu\mu}) \propto \exp\left(-\frac{H_{\mu\mu}^2}{L}\right)$ . The ensemble density i.e. the JPDF of the matrix elements of eq. (1) can now be written as

$$\rho_1(H) \propto \prod_{\mu} \exp\left(-\frac{H_{\mu\mu}^2}{L}\right) \prod_{\mu < \nu} \exp\left[-\left(1 + \frac{f_{\mu\nu}}{b^2}\right) \frac{H_{\mu\nu}^2}{2}\right], \quad (2)$$

where,  $\mu, \nu$  correspond to only connected pairs. For later reference, we rewrite eq.(2) as

$$\rho(H) = \mathcal{N} \exp \left[ - \sum_{\mu, \nu} \frac{1}{2v_{\mu\nu}} (H_{\mu\nu} - b_{\mu\nu})^2 \right] \quad (3)$$

with  $v_{\mu\nu} = \langle (H_{\mu\nu})^2 \rangle - \langle H_{\mu\nu} \rangle^2$  and  $b_{\mu\nu} = \langle H_{\mu\nu} \rangle$  and  $\mathcal{N}$  is the normalization constant. A comparison of eq.(2) with eq.(3) gives

$$v_{\mu\mu} = L/2, \quad v_{\mu\nu} = \left( 1 + \frac{f_{\mu\nu}}{b^2} \right)^{-1}, \quad b_{\mu\nu} = 0. \quad (4)$$

With vanishing variance of the off-diagonal elements for  $b = 0$ , the system becomes classical (Poissonian) (as in the case for non-random  $\Gamma = 0$ ). For  $b \rightarrow \infty$  the system goes to the GOE limit (analogous to large non-random  $\Gamma$  case).

**(ii) Random-field Heisenberg model (RFHM):** The Hamiltonian in this case describes the dynamics of  $L$  spin 1/2 particles on a one dimensional lattice in a random magnetic field,

$$H = \sum_{k=1}^L [J (S_k^x S_{k+1}^x + S_k^y S_{k+1}^y) + D S_k^z S_{k+1}^z - h_k S_k^z], \quad (5)$$

where  $2S^x, 2S^y, 2S^z$  are Pauli matrices,  $J$  is a constant which sets the energy scale,  $D$  is the anisotropy parameter, and the fields  $h_i$  are Gaussian random variables. The Hamiltonian conserves the total magnetization  $S_z^{tot} = \sum_{i=1}^L S_i^z$  even in presence of the disorder [16–18].

For a matrix representation of  $H$ , we choose the product state basis spanned by  $N = 2^L$  vectors of type  $|\mu\rangle \equiv \prod_{k=1}^L |\mu_k\rangle$  with each  $S_k |\mu_k\rangle = \mu_k |\mu_k\rangle$  with  $\mu_k = \pm 1/2$ . A state  $\Psi$  of  $H$  in this basis can be expressed as  $|\Psi\rangle \equiv \psi_\mu |\mu\rangle$ . For the entanglement analysis, we consider a bipartition of the spin-chain into two equal subparts, referring them as subsystem  $A$  and  $B$  with their local basis spaces as  $|a_\mu\rangle$  and  $|b_\mu\rangle$ . The basis state  $|\mu\rangle$  can then be written as the  $|\mu\rangle \equiv |a_\mu b_\mu\rangle$ . The components of  $|\Psi\rangle$  can now be written  $C_{a_\mu b_\mu}$ :  $\psi_\mu \equiv C_{a_\mu b_\mu} \equiv \langle a_\mu b_\mu | \Psi \rangle$ .

With onsite disorder, the diagonal elements of  $H$  are correlated random variables in the chosen basis. The nonzero off-diagonals are however non-random, equal to  $J/2$ . The JPDF of the matrix elements of the Hamiltonian in eq.(5) can then be written as

$$\rho_1(H) = C_1 \exp \left[ -\mathcal{H}_D^T B_D \mathcal{H}_D \right] \prod_{\mu < \nu} \delta \left( H_{\mu\nu} - \frac{J}{2} \right), \quad (6)$$

with  $C_1$  as the normalization constant,  $\mathcal{H}_D$  as a column vector of size  $N$ , consisting of the diagonals  $H_{\mu\mu} - \langle H_{\mu\mu} \rangle$  with  $H_{\mu\mu} \equiv \langle \mu | H | \mu \rangle$  of the Hamiltonian  $H$  in eq.(5), and  $B_D$  as the

precision matrix,  $B_D = \Sigma_D^{-1}$ , where  $\Sigma_D$  is the  $N \times N$  covariance matrix of the elements in  $\mathcal{H}_D$ :  $\Sigma_{D;\mu\nu} = \langle H_{\mu\mu} H_{\nu\nu} \rangle - \langle H_{\mu\mu} \rangle \langle H_{\nu\nu} \rangle = \sum_{k=1}^L \mu_k \nu_k \langle h_k^2 \rangle$  (details discussed in the supplementary file [11]). Assuming  $\langle h_k^2 \rangle = v^2$ , we then have  $\Sigma_{D;\mu\nu} = \beta_{\mu\nu} v^2$  with  $\beta_{\mu\nu} = \sum_{k=1}^L \mu_k \nu_k$  and  $v^2 = Lh^2/4$ . Again replacing  $\delta$ -functions by limiting Gaussians, the above  $\rho_1(H)$  can be rewritten as  $\rho_1(H) = \lim_{\Sigma_{\mu\nu, \mu'\nu'} \rightarrow 0} \rho(H)$  where

$$\rho(H) = C_1 \exp[-\mathcal{H}^T B \mathcal{H}] \quad (7)$$

$$= C_2 \exp \left[ - \sum_{\mu\nu; \mu'\nu'} B_{\mu\nu; \mu'\nu'} H_{\mu\nu} H_{\mu'\nu'} - A_{\mu\nu} H_{\mu\nu} \right] \quad (8)$$

with  $\mathcal{H}$  as a column vector of size  $M = N(N+1)/2$ , consisting of all diagonals and upper off-diagonals elements  $H_{\mu\nu} - \langle H_{\mu\nu} \rangle$  and  $B = \Sigma^{-1}$  where  $\Sigma$  is the new covariance matrix of size  $M \times M$ :  $\Sigma_{\mu\nu, \mu'\nu'} = \langle H_{\mu\nu} H_{\mu'\nu'} \rangle - \langle H_{\mu\nu} \rangle \langle H_{\mu'\nu'} \rangle$ . Here  $A_{\mu\nu} = -2 \sum_{\mu'\nu'} B_{\mu\nu, \mu'\nu'} \langle H_{\mu'\nu'} \rangle$ . As discussed in detail in the supplementary file [11], we have

$$\begin{aligned} B_{\mu\mu, \nu\nu} &= \left( \frac{1}{v^2} \right) \beta_{\mu\nu}^{-1}, & B_{\mu\nu, \mu\nu} &= 0 & \mu &\neq \nu, \\ A_{\mu\nu} &= - \left( \frac{2D}{v^2} \right) \alpha_\nu \beta_{\mu\nu}^{-1}, & \langle H_{\mu\nu} \rangle &= D \alpha_\mu \delta_{\mu\nu} + \frac{J}{2} (1 - \delta_{\mu\nu}) \end{aligned} \quad (9)$$

The system, eq. (5), exhibits an ergodic phase (delocalized wavefunctions) for low disorder and a localized phase as the disorder strength becomes large. This is consistent with its accepted ensemble representation:  $\rho(H)$  corresponds to a Gaussian orthogonal ensemble (GOE) in low disorder limit which has delocalized eigenfunctions, and, a Poisson ensemble in strong disorder limit with localized eigenfunctions.

**(iii) Two body Hamiltonian: interaction with/without disorder:** The dynamics of 2 electrons in a lattice of  $\mathcal{N}$  sites described by the Hamiltonian

$$H = \sum_{k,l;\sigma} V_{kl} a_{k\sigma}^\dagger a_{l\sigma} + \sum_{k,\sigma,\sigma'} U_k a_{k\sigma}^\dagger a_{k\sigma} a_{k\sigma'}^\dagger a_{k\sigma'} \quad (10)$$

with  $|k\sigma\rangle = a_{k\sigma}^\dagger |0\rangle$ ,  $k = 1 \rightarrow N$  as the  $N$ -dimensional site basis ( $N = 2\mathcal{N}$ ),  $\sigma, \sigma' = \pm 1$  referring to two spin states of the electron. The strength of the onsite interaction is  $U_k$ , with  $V_{kk} = \varepsilon_k$  as the on site energy and  $V_{kl}$  the hopping element between sites  $k, l$ :  $V_{kl} \neq 0$  if  $k, l$  are neighbouring sites and zero otherwise. The standard basis for analysis in this case is the

antisymmetrized two particle product basis of size  $N_2 = N(N - 1)/2$  with basis states as  $|k\sigma_1; l\sigma_2\rangle = \frac{1}{\sqrt{2}} (|k\sigma_1\rangle \cdot |l\sigma_2\rangle - |l\sigma_2\rangle \cdot |k\sigma_1\rangle)$  with  $|k\sigma\rangle$  as the single particle state at the site  $k$  for a particle with spin  $\sigma$ . This leads to a  $N_2 \times N_2$  Hermitian matrix representation of  $H$  with a general matrix element  $\langle k\sigma_1; l\sigma_2 | H | i\sigma_3; j\sigma_4 \rangle$  becomes, with  $|\mu\rangle \equiv |k\sigma_1; l\sigma_2\rangle$ ,  $|\nu\rangle \equiv |i\sigma_3; j\sigma_4\rangle$ , and  $H_{\mu\mu} = V_{kk} + V_{ll} + U_k \delta_{kl} (1 - \delta_{\sigma_1\sigma_2})$ ,  $H_{\mu\nu} = (V_{ik}\delta_{jl} + V_{jl}\delta_{ik}) \delta_{\sigma_1\sigma_3} \delta_{\sigma_2\sigma_4}$ . Here  $V_{kl}$  or  $U_k$  can be random due to error in their exact determination or presence of disorder. Further, with  $1 \leq k, l \leq N$ , the size  $N_2$  of the antisymmetrized basis is  $N(N - 1)/2$ . Contrary to previous case, an analysis of this case can provide information about the two particle entanglement.

Based on the nature of interaction strengths (single or two particle),  $H$  can be a sparse or dense random matrix. For clear exposition of our ideas, here we consider the case with random independent interaction parameters  $U_k$ , on-site energies  $V_{kk} = 0$ , a hopping strength  $t$  between nearest neighbor (n.n.) sites, hopping strength  $t_1$  between all other sites (choosing  $t_1 = 0$  later). The choice renders the diagonals  $H_{\mu\mu}$  uncorrelated, random (if  $k = l$ ,  $\sigma_1 \neq \sigma_2$ ). A choice of Gaussian distributed  $U_k$  with mean  $\langle U_k \rangle = U_0$  and variance  $w^2$  then results in a same distribution for all  $H_{\mu\mu}$  if  $k = l$ ,  $\sigma_1 \neq \sigma_2$ . Further, with  $H_{\mu\nu} = t e^{i\eta}$  as the hopping element, a choice of both  $t$  and  $\eta$  leaves  $H_{\mu\nu}$  non-random. The ensemble density for  $H$  can now be given as

$$\rho_2(H) = \prod_{k=l, s_1 \neq s_2}^{\mu} e^{-\frac{(H_{\mu\mu} - U_0)^2}{2w^2}} \prod_{s_1=s_2}^{\mu} \delta(H_{\mu\mu}) \prod_{\substack{\mu, \nu \\ \text{connected}}}^N \delta(H_{\mu\nu} - t e^{i\eta}) \prod_{\substack{\mu, \nu \neq \\ \text{connected}}}^N \delta(H_{\mu\nu})$$

Proceeding as in previous case,  $\rho_2(H)$  can now be expressed as a multi-parametric Gaussian ensemble of complex Hermitian matrices  $\rho_2(H) = \lim_{v_{\mu\nu} \rightarrow 0} \rho(H)$  where the notation  $\lim_{v_{\mu\nu} \rightarrow 0}$  implies the limit taken for all  $v_{\mu\nu}$  with  $\mu \neq \nu$ .

$$\rho(H) = \mathcal{N} \exp \left[ - \sum_{\mu, \nu; s} \frac{1}{2v_{\mu\nu; s}} (H_{\mu\nu; s} - b_{\mu\nu; s})^2 \right] \quad (11)$$

with subscript "s" referring to real ( $s = 1$ ) or imaginary part ( $s = 2$ ) of the variable and  $\mathcal{N}$  as the normalization constant. A comparison of eq. (11) with eq. (11) now gives  $v_{\mu\mu} = w^2 d_{|\sigma_1 - \sigma_2|}$ ,  $v_{\mu\nu} = \xi^2 c_{|\mu - \nu|}$ ,  $b_{\mu\mu} = U_0 d_{|\sigma_1 - \sigma_2|}$  for  $k = l$ ,  $\sigma_1 \neq \sigma_2$  and  $b_{\mu\nu} = \langle H_{\mu\nu} \rangle = t e^{i\eta} c_{|\mu - \nu|}$  for  $j = l$  and  $i, k = n.n.$  and  $b_{\mu\nu} = t c_{|\mu - \nu|}$  for  $i = k$  and  $j, l = n.n.$  Here  $d_{|\sigma_1 - \sigma_2|} = 1$ , if  $\sigma_1 \neq \sigma_2$ , otherwise it is zero, and  $c_{|\mu - \nu|} = 1$  for all  $\mu, \nu$  pairs.

Recalling that  $\mu$  is a 2-body product basis i.e.  $|\mu\rangle \equiv |ks_1; ls_2\rangle$ , we can rewrite it in standard bipartite basis notation:  $|\mu\rangle \equiv |a, b\rangle$  with  $|a\rangle \equiv |ks_1\rangle$  and  $|b\rangle \equiv |ls_2\rangle$  and  $a =$

$1, 2, \dots, N$ ,  $b = 1, 2, \dots, N$ . This helps to rearrange eigenfunction components in form of a matrix  $C$ , with its elements  $C_{ab} \equiv U_{\mu\nu}$  and  $\sum_{\mu} \equiv \sum_{a,b} s_2$  or zero (if  $s_1 = s_2$ ).

In general, with non-zero on-site energies  $V_{kk}$ , the diagonals  $H_{\mu\mu}$  need not be all uncorrelated for all system conditions. It is therefore relevant to analyze the correlated ensembles of Hamiltonians but is technically non-trivial[19]. For example, for a pair-wise correlations among the diagonals, the appropriate ensemble density becomes

$$\rho(H) = \mathcal{N} \exp \left[ - \sum_{\mu\nu, s; \mu', \nu', s'} b_{\mu\nu, s; \mu' \nu' s'} H_{\mu\nu; s'} H_{\mu' \nu'; s} - a_{\mu\nu} H_{\mu\nu; s} \right]. \quad (12)$$

#### IV. VARIATION OF SYSTEM PARAMETERS: RESPONSE OF HAMILTONIAN ENSEMBLE DENSITY

In contrast to the eigenvalues, the eigenstates of an operator are basis dependent. With primary focus on the eigenstates dynamics in this work, it is relevant to choose an appropriate basis for the Hamiltonian matrix representation. In case a Hamiltonian has discrete global symmetries, an appropriate basis for its representation is a symmetry resolved basis. The latter leads to a block diagonal structure and ensures that each block has non-degenerate eigenvalues. With physical properties of different blocks uncorrelated, it is then sufficient to consider an ensemble of symmetry resolved blocks, with different members of the ensemble sharing the same set of global constraints (e.g., quantum numbers, symmetry conditions and conservation laws). For clear exposition of our ideas without loss of generality, here we consider a Hamiltonian with non-degenerate eigenvalues.

A change in system conditions results in a variation of matrix elements of  $H$  and thereby its ensemble density which in turn manifests on the eigenfunction components in the basis space and their statistical behavior. The evolution of the ensemble densities  $\rho(H)$  given by eq.(3), eq.(8), eq.(11) or eq.(12) with changing ensemble parameters and their complexity parameter formulation is discussed in detail in [10, 19, 20]. To avoid confusion with state ensemble used in this work, hereafter we refer  $\rho(H)$  as the Hamiltonian ensemble. For purpose of clarity, here we briefly review the complexity parameter formulation for the ensemble described by eq.(3).

As discussed in previous studies [19–22], a specific combination  $T\rho \equiv \sum_{\mu < \nu} [(g_{\mu\nu} - 2\gamma v_{\mu\nu}) \frac{\partial \rho}{\partial v_{\mu\nu}} - \gamma b_{\mu\nu} \frac{\partial \rho}{\partial b_{\mu\nu}}]$  of first order variation of the ensemble parameters  $v_{\mu\nu; s} \rightarrow v_{\mu\nu; s} + \delta v_{\mu\nu; s}$

and  $b_{\mu\nu;s} \rightarrow b_{\mu\nu;s} + \delta b_{\mu\nu;s}$  over time would lead to a Brownian dynamics in Hermitian matrix space, starting from an arbitrary initial condition and with a stationary ensemble as the equilibrium limit:  $T\rho = L\rho$  where  $L \equiv \sum_{\mu,\nu} \frac{\partial}{\partial H_{\mu\nu;s}} \left[ \frac{g_{\mu\nu}}{2} \frac{\partial}{\partial H_{\mu\nu;s}} + \gamma H_{\mu\nu;s} \right]$  with  $g_{\mu\nu} = 2$  or  $1$  for  $\mu = \nu$  and  $\mu \neq \nu$ , respectively. A transformation of the set  $\{v_{\mu\nu}, b_{\mu\nu}\}$  to another set  $\{t_1, t_2, \dots, t_M\}$  however reduces the multi-parametric dynamics in the ensemble space to a single parameter dynamics, say with respect to  $t_1$ , while others, i.e,  $t_2 \dots t_M$  remaining constant throughout the evolution,

$$\frac{\partial \rho}{\partial t_1} = L \rho, \quad (13)$$

where, The above condition can be fulfilled by three possible ways (details discussed in supplemental material [11]):

$$\text{Case I} \quad Tt_1 = 1, Tt_n = 0 \quad n > 1, \quad \frac{\partial \rho}{\partial t_\alpha} = 0 \quad \forall \alpha > 1, \quad (14)$$

$$\text{Case II} \quad Tt_1 = 1, \frac{\partial \rho}{\partial t_\alpha} = 0 \quad \forall \alpha > 1 \quad (15)$$

$$\text{Case III} \quad Tt_1 = 1, Tt_n = 0 \quad \forall n > 1, \quad (16)$$

The parameters  $t_1, \dots, t_M$  for each one of the above cases can be obtained by solving the characteristic set of equations  $\frac{dy_{kl;s}}{A_{kl;s}} = \frac{dx_{kl;s}}{B_{kl;s}} = \frac{dt_\alpha}{\delta_{\alpha 1}}$  with  $k, l = 1 \rightarrow N$ . Here  $M$  corresponds to total number of ensemble parameters participating in evolution. Here  $M = 2N^2$  for all of them varying,  $M < 2N^2$  in case  $\frac{\partial \rho_1}{\partial y_{kl}} = 0$  or  $\frac{\partial \rho_1}{\partial x_{kl}} = 0$  for some  $y_{kl}$  or  $x_{kl}$ , with  $k, l$  arbitrary. For example, for the case with  $x_{kl} = 0$  ( $\forall k, l$ ), we have  $M = 2N^2$ .

The transformation maps the JPDF  $\rho$  in eq.(3) to  $\rho(H; t_1, t_2, \dots, t_M)$  with  $t_1, t_2, \dots, t_M$  given by a set of characteristic equations [20]

$$\frac{dv_{\mu\nu;s}}{f_{\mu\nu;s}} = \dots = \frac{dv_{\mu\nu;s}}{f_{\mu\nu;s}} = \frac{db_{\mu\nu;s}}{b_{\mu\nu;s}} = \frac{dt_\alpha}{\delta_{\alpha 1}} \quad (17)$$

with  $f_{\mu\nu;s} \equiv (g_{\mu\nu} - 2\gamma v_{\mu\nu;s})$ . A general solution of the above equation for  $t_1$  can be given as

$$t_1 = -\frac{1}{2M\gamma} \sum_{s=1}^{\beta} \sum_{\mu \leq \nu} \left( q_{\mu\nu} \ln |g_{\mu\nu} - 2\gamma v_{\mu\nu;s}| + p_{\mu\nu} \ln |b_{\mu\nu;s}|^2 \right) + const. \quad (18)$$

with  $q_{\mu\nu}$  and  $p_{\mu\nu}$  as arbitrary constants dependent on initial conditions, and  $\beta$  is the Dyson's index, which is 1 (2) for real-symmetric (complex-Hermitian) matrices. Choosing  $q_{\mu\nu} = 1, p_{\mu\nu} = 1$  and with  $t_1 \equiv Y$ , we have

$$Y = -\frac{1}{2M\gamma} \ln \left[ \prod_{s=1}^{\beta} \prod_{\mu \leq \nu} |g_{\mu\nu} - 2\gamma v_{\mu\nu;s}| |b_{\mu\nu;s}|^2 \right] + \text{const.} \quad (19)$$

Similarly  $t_2, \dots, t_M$  can be obtained by solving the eq.(17) for  $\alpha > 1$ . As their explicit forms are not needed for further analysis, we omit the related details here. Also, we note that  $t_2, \dots, t_M$  remain not only constants of the evolution described by eq.(13), they can also be chosen as the basis constants [8]. The product in eq.(19) is over  $M$  non-zero terms. As clear from the above,  $Y$  turns out to be an average distribution parameter, a measure of average uncertainty of system, also referred as the ensemble *complexity parameter*.

The complexity parameter formulation for eq.(8), i.e., ensemble densities with pairwise matrix elements correlations can be derived by following the similar steps as mentioned above. The evolution equation for  $\rho(H)$  again turns out to be the same form as eq.(13) but the parameters  $t_1, \dots, t_M$  are now different and are determined by following set of characteristics equations

$$\frac{dB_{\mu\nu,\mu'\nu'}}{f_{\mu\nu,\mu'\nu'}} = \dots = \frac{dA_{\mu\nu}}{f_{\mu\nu}} = \frac{dt_\alpha}{\delta_{\alpha 1}} \quad (20)$$

where,

$$\begin{aligned} f_{\mu\nu} &= \gamma A_{\mu\nu} - \sum_{\mu'\nu'} g_{\mu'\nu'} C_{\mu\nu,\mu'\nu'} \\ f_{\mu\nu,\mu'\nu'} &= \gamma C_{\mu\nu,\mu'\nu'} - \frac{1}{2} \sum_{\mu''\nu''} g_{\mu''\nu''} C_{\mu\nu,\mu''\nu''} C_{\mu'\nu',\mu''\nu''}, \end{aligned} \quad (21)$$

where,  $C_{\mu\nu,\mu'\nu'} = (1 + \delta_{\mu\mu'}\delta_{\nu\nu'})B_{\mu\nu,\mu'\nu'}$ , and  $A_{\mu\nu}$  and  $B_{\mu\nu,\mu'\nu'}$  are defined in eqs.(9). A solution of the above equation for  $t_1$  can be given as

$$t_1 = \sum_{\mu\nu,\mu'\nu'} q_{\mu\nu,\mu'\nu'} \int \frac{dB_{\mu\nu,\mu'\nu'}}{f_{\mu\nu,\mu'\nu'}} + \sum_{\mu\nu} q_{\mu\nu} \int \frac{dA_{\mu\nu}}{f_{\mu\nu}} + \text{constant} \quad (22)$$

with  $q_{\mu\nu,\mu'\nu'}$  and  $q_{\mu\nu}$  as arbitrary constants dependent on initial conditions, and, as before, can be chosen to be 1 for simplicity.

## V. SCHMIDT EIGENVALUES DYNAMICS WITH CHANGING SYSTEM CONDITIONS

An eigenstate  $U_\nu$  of the Hamiltonian  $H$  corresponding to an energy  $e_\nu$  can in principle be obtained by solving the eigenvalue equation  $HU_\nu = e_\nu U_\nu$ ,  $\nu = 1 \rightarrow N$ . Contrary to

the eigenvalues, the behavior of an eigenfunction depends on the basis in which the latter is represented. As the suitable basis for the bipartite entanglement analysis of an eigenfunction is the bipartite basis, we express  $U_\nu$  in the  $N = N_A N_B$ -dimensional product basis  $|a_k b_l\rangle$  with  $k = 1 \rightarrow N_A, l = 1 \rightarrow N_B$  with  $C_{\nu;kl}$  as the components:

$$U_\nu = \sum_{k=1}^{N_A} \sum_{l=1}^{N_B} C_{\nu;kl} |a_k b_l\rangle. \quad (23)$$

With the components of  $U_\nu$  now labelled by two indices, it is appropriate to represent them in a  $N_A \times N_B$  matrix form  $C_\nu$  referred as a state matrix. (Thus, in contrast to the eigenfunction matrix  $U$  which consists of  $U_\nu$ ,  $\nu = 1 \rightarrow N$  as its columns,  $C_\nu$  represents a single eigenfunction  $U_\nu$ ). With further analysis confined to a single eigenfunction, hereafter the subscript  $\nu$  in  $C_\nu$  will be suppressed for clarity purposes unless necessary.

### A. Dynamics of the eigenfunction components

As the eigenvalue equation implies, a randomization of  $H$  results in a fluctuations of the eigenvalues and eigenfunctions. The joint probability density function (JPDF) of the latter is related to the probability density of  $H$  matrix as follows

$$P(e_1, \dots, e_N, U_1, \dots, U_N) \prod_{\nu=1}^N (de_\nu dU_\nu) = \rho(H) DH, \quad (24)$$

A complexity parameter based formulation of  $\rho(H)$  along with the above relation can then be used to derive a similar formulation for the statistics of the eigenfunctions and eigenvalues. With our interest in a single eigenfunction dynamics in a bipartite basis, we confine the discussion here to the joint probability density function (JPDF) of the components  $C_{kl}$  of  $U_\nu$  and proceed as follows. The JPDF  $P_c(C) \equiv P_c(C_{11}, C_{12}, \dots, C_{N_N})$  of the components  $C_{kl}$  of  $U_\nu$  is defined as

$$P_c(C) = \int \prod_{k,l=1}^{N_A, N_B} \delta(C_{kl} - C_{kl}(H)) \delta(C_{kl}^* - C_{kl}^*(H)) \rho(H) dH. \quad (25)$$

Differentiating the above equation with respect to  $Y$ , followed by substitution of eq.(13) and repeated partial integration then leads to

$$\frac{\partial P_c}{\partial \Lambda_\psi} = (L + L^*) P_c \quad (26)$$

where

$$L \equiv \sum_{k,l} \frac{\partial}{\partial C_{kl}} \left( \sum_{m,n} \frac{\partial(\delta_{mk}\delta_{nl} - C_{kl}C_{mn}^*)}{\partial C_{mn}^*} + (N-1)C_{kl} \right) \quad (27)$$

and  $\Lambda_\psi$  is the rescaled evolution parameter

$$\Lambda_\psi(e) = \frac{(Y - Y_0)}{\Omega_e^2} \quad (28)$$

with  $\Omega_e$  as a system-specific energy scale around energy  $e$  beyond which the eigenvalues are uncorrelated. Assuming  $N_k$  as the number of eigenvalues in the range and  $\Delta_{local}(e)$  as the local mean level spacings at the energy  $e$ , we can write  $\Omega_e(e) = N_k \Delta_{local}(e)$ . Intuitively  $N_k$  expected to be related to the inverse participation ratio  $I_2 = \frac{1}{N} \sum_{n=1}^N |\psi_n|^4$  at energy  $e$ , i.e.  $N_k \propto N \langle I_2 \rangle$ . This suggests that

$$\Omega_e \approx \kappa N \langle I_2(e) \rangle \Delta_{local}(e) \quad (29)$$

with  $\kappa$  as the proportionality constant with units of  $\langle I_2(e) \rangle$  and  $\Delta_{local}(e)$  as the local mean level spacing at energy  $e = e_k$ .

Eq.(26) describes the  $\Lambda_\psi$  governed evolution of the JPDF of the state matrix elements  $C_{kl}$  for a fixed system size  $N$  starting from for an arbitrary initial condition. Previously an evolution equation for the state matrix elements representing an arbitrary *engineered quantum state* in a bipartite basis was derived in [7–9]. The distribution  $P_c(C)$  in these studies was assumed to be a multiparametric Gaussian ensemble with independent matrix elements; assuming that the state components are described only by the first two moments and are uncorrelated; such a distribution for a state matrix ensemble follows directly by invoking maximum entropy hypothesis. Interestingly the equation in the *engineered state case* can again be written in the same form as eq.(26) but the generator  $L$  differs in important details:  $L \equiv \sum_{mk} \frac{\partial}{\partial C_{kl}} \left( \frac{\partial}{\partial C_{kl}^*} + C_{kl} \right)$ . We note the missing correlation terms between components can not simply be introduced by consideration of a correlated Gaussian ensemble of state matrices.

## B. Dynamics of the Schmidt eigenvalues

As mentioned in section II, the entanglement entropy  $R_1$  corresponds to the von Neumann entropy of the reduced density matrix  $\rho_A = CC^\dagger$  and can be determined, in principle from

the Schmidt eigenvalues. Following from the above definition, a randomization of  $C$ -matrix is expected to cause the fluctuations of  $\lambda_n$ , thereby making it relevant to derive a theoretical formulation of the JPDF  $P(\lambda) \equiv P(\{\lambda_i\}) \equiv P(\lambda_1, \dots, \lambda_{N_A})$ . A prior knowledge of the latter can then be used to derive the ensemble average of  $R_1$  as well as its higher order moments.

We proceed as follows. A comparison of eq.(26) with standard Fokker-Planck equation gives the  $\Lambda$ -dependent moments of the  $C$ -elements, i.e.,  $\langle C_{kl} \rangle, \langle C_{kl} C_{mn}^* \rangle$  and thereby the moments of the matrix elements  $\rho_{A;mn} = \sum_{k=1}^{N_A} C_{mk} C_{nk}^*$  (details given in [11]). The latter along with the second order perturbation theory for Hermitian matrix eigenvalues then leads to the  $\Lambda$ -dependent moments of  $\lambda_n$ . Assuming Markovian dynamics for the latter, a substitution of their moments in standard Fokker-Planck equation then leads to evolution equation for  $P(\lambda)$  with  $\Lambda_\psi$  as the evolution parameter,

$$\frac{\partial P}{\partial \Lambda_\psi} = \mathcal{L}P - \mathcal{L}_{cor}P \quad (30)$$

where

$$\mathcal{L} \equiv \sum_{n=1}^{N_A} \left[ \frac{\partial^2 (\lambda_n P)}{\partial \lambda_n^2} - \beta \frac{\partial}{\partial \lambda_n} \left( \sum_{\substack{m=1 \\ m \neq n}}^{N_A} \frac{\lambda_n}{\lambda_n - \lambda_m} + \nu_e - \eta \lambda_n \right) \right] \quad (31)$$

$$\mathcal{L}_{cor} \equiv \sum_{m,n=1}^{N_A} \frac{\partial^2}{\partial \lambda_n \partial \lambda_m} [(\lambda_n \lambda_m) P] \quad (32)$$

with  $\eta = \frac{N_A N_B}{2}$  and  $\nu_e = \frac{N_A - N_B - 1}{2}$ . We note that, with presence of an additional term, i.e.,  $\mathcal{L}_{cor}P$ , eq.(30) differs from the one derived in previous work for the engineered state ensemble [7]. The additional term indicates a crucial difference from the previous study: it reflects the effect of correlations among eigenfunction components present in a quantum state derived from a physical Hamiltonian; this aspect was not considered in the engineered quantum states discussed in previous works [7–9].

### C. Mapping of the ensemble parameter space to complexity space: significance

As discussed in section IV, we map the evolution of the ensemble density  $\rho(H)$  due to changing ensemble parameters to another  $M$ -dimensional parameter space consisting of  $t_1, t_2, \dots, t_M$  as variables and referred as "complexity space" (to distinguish it from original ensemble parameter space). The evolution in complexity space however occurs along the

curves along which only  $Y \equiv t_1$  varies, with  $t_2, \dots, t_M$  remaining constants. These constants can therefore be determined from the initial condition on  $\rho(H)$ . The above in turn leads to the evolution equations for the state matrix elements of a typical eigenstate of  $H$  and thereby for the Schmidt eigenvalues in the complexity parameter space (i.e Eq.(26) and Eq.(30) respectively). The reduction of the multiparametric dynamics to a single parametric one is useful not only for technical purposes but it also reveals a hidden web of connection as well as infinite range of universality classes of the eigenfunction statistics among the eigenstates of those Hamiltonians which can be represented by  $\rho(H)$ . This can be further elucidated as follows.

For a fixed  $N_A, N_B$ , the solution of Eq.(30) depends on  $\Lambda_\psi$  only, the latter a function of ensemble parameters which in turn are governed by underlying system conditions. This implies an analogy of the solutions for two different states if (i) both start from statistically similar initial conditions, (ii) share same  $\Lambda_\psi$  values, (iii) belong to same or different Hamiltonians represented by the ensemble  $\rho(H)$  although their ensemble parameters can in general be different. In addition, as a change in the system parameters for finite  $N$  can change  $\Lambda_\psi$  continuously between 0 and  $\infty$ , this predicts the existence of an infinite range of universality classes of the JPDF characterized by continuous values of  $\Lambda_\psi$  between 0 and  $\infty$ .

Additional important insight can be gained by noting that  $\Lambda_\psi$  itself is a function of  $N$  through both  $Y - Y_0$  as well as  $\Omega_e$ . A subtle competition between the  $N$ -dependence of the two scales, especially in large  $N$  limit, can then play an important role in determining the statistics. For example, assuming  $Y - Y_0 \propto N^s$  and  $\Omega_e \propto N^q$ , with  $s, q$  as the system-dependent constants, gives  $\Lambda_\psi \propto N^{s-2q}$ . As  $N \rightarrow \infty$ , therefore,  $\Lambda_\psi \rightarrow \infty$  for the system conditions leading to  $s > 2q$  and thereby to the uniformly distributed components of the Haar-unitary state. Similarly, for the system conditions leading to  $s < 2q$ ,  $\Lambda_\psi \rightarrow 0$  and the state ensemble remains stuck at its initial state. If however a specific combination of the prevailing system conditions lead to  $s = 2q$ , this renders  $\Lambda_\psi$  independent of  $N$ ; referring the corresponding  $\Lambda_\psi$  value as  $\Lambda^*$ , it would then remain finite even in the  $N \rightarrow \infty$  limit [10]:

$$\Lambda^* = \lim_{N \rightarrow \infty} \Lambda_\psi \neq 0, \infty. \quad (33)$$

The statistics at  $\Lambda^*$  remains therefore different from the two end points (i.e.,  $\Lambda = 0$  and  $\infty$ ) even in infinite size limit and can be referred as critical. Indeed, based on the complexity of the system, more than one set of system parameters may exist, resulting in more than

one  $\Lambda^*$  and thereby multiple critical statistics intermediate between the initial state and Haar-unitary ensembles. In infinite size limit, Eq.(30) therefore indicates the existence of discrete universality classes for the eigenfunction statistics, each characterized by a distinct  $\Lambda^*$ . The explicit appearance of size  $N$  in Eq.(26) (in addition to its implicit appearance through  $\Lambda$ ), however, suggests that the statistics at  $\Lambda^*$  for finite  $N$  is different from that of infinite  $N$ .

As discussed in [19, 22] in detail, the eigenvalue dynamics of the ensemble  $\rho(H)$  with changing ensemble parameters can also be described by a mathematical formulation governed by a single function of all ensemble parameters. The latter, referred as the *spectral complexity parameter*, is defined as  $\Lambda_e(e) = \frac{(Y-Y_0)}{\Delta_{local}^2}$  [10, 19]. Here again the competition between  $N$ -dependence of  $Y - Y_0$  and  $\Delta_{local}$  leads to a critical spectral statistics at energy  $e$  if

$$\Lambda_e^* \equiv \lim_{N \rightarrow \infty} \Lambda_e(e) = \text{finite.} \quad (34)$$

A comparison of the above equation with eq.(28) gives

$$\Lambda_\psi(Y - Y_0; e) = \chi \Lambda_e(Y - Y_0; e), \quad (35)$$

where  $\chi$  is in general a function of  $Y - Y_0$  as well as energy  $e$  (see Section SIII of the Supplementary Material),

$$\chi(Y - Y_0, e) \approx \frac{\Delta_{local}^2}{\Omega_e^2} = \frac{1}{\kappa^2 N^2 \langle I_2 \rangle^2} \quad (36)$$

To distinguish it from  $\Lambda_e$  and  $Y - Y_0$ , hereafter we refer  $\Lambda_\psi$  as the *strength complexity parameter*. The above relation implies significant correlations among eigenvalues and eigenfunctions in the critical regime and is in agreement with previous statistical studies of the complex Hamiltonians.

Eq.(35) implies the existence of a finite size scaling and a multifractal behavior of the eigenfunction statistics at the critical point, with scaling exponents (referred to as critical exponents or multifractal dimensions) dependent on the system parameters [10]. As  $\Lambda_e$  is sensitive to system specifics, the critical (multifractal) exponents can vary from system to system. The existence of a critical spectral statistics and multifractal behavior of the eigenstates however requires a specific set of system conditions conspiring with each other and leading to a size-independent  $\Lambda$  (a more detailed discussion of  $\Lambda$  is included in the supplementary material [11]).

As eq.(35) indicates, the rescaling of  $Y - Y_0$  leads to  $e$ -dependence of  $\Lambda_\psi$ , thereby implying a lack of translational invariance in the statistical behavior along the spectral axis (also referred as the non-stationarity). It is important to emphasize here the difference between the mean level density of state  $R(e) = \langle \sum_n \delta(e - e_n) \rangle$  and  $R_{local}(e)$ : in contrast to the former,  $R_{local}$  corresponds to the weighted density of states, with weight corresponding to those eigenstates at energy  $e$  which also occupy same basis space; this is discussed in detail in [11].

## VI. COMPLEXITY PARAMETER FORMULATION OF THE ENTANGLEMENT MEASURES

In this section, we derive the complexity parameter formulation of the average behavior as well as the variance of the standard measure used to quantify entanglement, namely the von Neumann entropy. To avoid cluttering of the symbols, we hereafter suppress the subscript  $\psi$  from  $\Lambda_\psi$  and restore it only if necessary for clarity.

### A. von Neumann entropy statistics

The ensemble averaged von Neumann entropy  $\langle R_1 \rangle$  can be defined as

$$\langle R_1 \rangle = \int \left( - \sum_n \lambda_n \log \lambda_n \right) P(\lambda) D\lambda. \quad (37)$$

Differentiating the above equation with respect to  $\Lambda$ , followed by substitution of eq.(30) and simplifying by partial integration (details discussed in [7] and also in [11]), we have

$$\frac{\partial \langle R_1 \rangle}{\partial \Lambda} = \alpha + \frac{N_B}{2} \langle R_0 \rangle - \frac{N_A N_B}{2} \langle R_1 \rangle. \quad (38)$$

with  $\alpha = 1 - \frac{N_A(N_A+1)}{2}$  and  $R_0 = - \sum_n \log \lambda_n$  with  $\langle R_0 \rangle$  as its ensemble average.

The above equation describes the  $\Lambda$ -governed growth of average von Neumann entropy, from an arbitrary initial state at  $\Lambda = 0$  (equivalently  $Y = Y_0$ ). As  $R_0 \rightarrow \infty$  under separability condition (i.e.  $\lambda_n = 0$  for all  $n = 1 \rightarrow N$  except one of them), the above implies a rapid variation of  $\frac{\partial \langle R_1 \rangle}{\partial \Lambda}$  for  $\Lambda$  near 0 if the initial state ensemble is separable. Further, with  $\frac{\partial \langle R_1 \rangle}{\partial \Lambda} \rightarrow 0$  and  $\langle R_0 \rangle \rightarrow N_A \log N_A + \frac{N_A^2}{2N_B}$  as  $\Lambda \rightarrow \infty$  [7], the above equation gives  $\langle R_1 \rangle = \log N_A - \frac{N_A}{2N_B}$  for large  $\Lambda$ . The latter agrees with the Page limit [23] for the ergodic

states; (we recall that the state  $\Psi$  approaches ergodic limit as  $\Lambda \rightarrow \infty$ ). A change from  $\frac{\partial \langle R_1 \rangle}{\partial \Lambda} \rightarrow 0$  to  $\infty$  is expected to take place at a finite  $\Lambda$  value when  $\langle R_0 \rangle$  becomes finite and is of the same order as that of  $\langle R_1 \rangle$ . Indeed, as our numerics indicated, the change occurs where the correlation between  $R_0$  and  $R_1$  is maximum.

A general solution for eq.(38) for arbitrary  $\Lambda$  and an arbitrary initial condition can be given as

$$\langle R_1 \rangle(\Lambda) = \langle R_1 \rangle(0) e^{-\frac{N\Lambda}{2}} + \frac{2\alpha}{N} \left(1 - e^{-\frac{N\Lambda}{2}}\right) + \frac{N_B}{2} e^{-\frac{N\Lambda}{2}} \int_0^\Lambda \langle R_0 \rangle e^{\frac{N\Lambda}{2}} d\Lambda \quad (39)$$

The above solution however requires a prior knowledge of  $\Lambda$ -dependence of  $\langle R_0 \rangle$  for finite  $\Lambda$ . In addition,  $R_0 = -\sum_n \log \lambda_n$  is infinite in the separability limit (one of the eigenvalues as 1 and rest zero); the latter can not then be considered as an initial condition to determine  $\langle R_1 \rangle(\Lambda)$ . It is however possible to choose a weak separability limit as an initial condition at  $\Lambda = 0$ ; this can be explained as follows. From its definition,  $R_0$  become singular even if only one of the eigenvalues is zero. With changing system conditions however the eigenvalues evolve increasingly becoming nonzero. But  $R_0$  become finite only when one of the eigenvalues is  $1 - N_A^{-q}$  and rest of them are  $\sim N_A^{-(q+1)}$  with  $q > 1$ . This gives  $R_0 \sim (q+1)N_A \log N_A$  and  $R_1 \sim N_A^{-q}(1 - N_A^{-q}) + qN_A^{-q}(N_A - 1) \log N_A$ . Thus, taking the initial condition at  $\Lambda = 0$  as one of the eigenvalues  $1 - N_A^{-q}$  and rest of them as  $\sim N_A^{-(q+1)}$ , we have  $\langle R_1 \rangle(0) = 0$  with  $q > 1$ .

Following from the above, a particular solution of eq.(38) for arbitrary  $\Lambda$ , with weak separability initial condition, can be given as

$$\langle R_1 \rangle(\Lambda) = \alpha_0 \left(1 - e^{-\frac{N\Lambda}{2}}\right), \quad (40)$$

with  $\alpha_0$  as the constant of integration. A substitution of eq.(40) in eq.(38) gives  $\alpha \approx \log N_A - \frac{N_A}{2N_B}$ ; this is consistent with expected  $\Lambda \rightarrow \infty$  limit of  $\langle R_1 \rangle(\Lambda)$ .

As clear from the above,  $\langle R_1 \rangle(\Lambda)$  rapidly changes from  $0 \rightarrow \log N_A$  near  $\Lambda \approx 2/N$ . Indeed, this is expected, with the  $\Lambda$ -value corresponding to a change of  $R_0$  from  $\infty$  to a finite value and  $R_1$  from 0 to its maximum limit, and can be explained as follows. At the separability limit, only one of the eigenvalues, say  $\lambda_1$ , is one and rest are zero. With changing system conditions however the eigenvalues evolve increasingly becoming nonzero; second order perturbation theory of Hermitian matrix spectrum gives  $\langle \delta \lambda_n \rangle = \beta \left[ -(N-1) \lambda_n + \sum_{m(\neq n)} \frac{\lambda_n + \lambda_m}{\lambda_n - \lambda_m} \right] \delta \Lambda$  (discussed in section III of supplemental material).

For a zero eigenvalue at  $\Lambda = 0$ , this implies  $\langle \delta \lambda_n \rangle \sim \frac{\delta \Lambda}{\Delta_\lambda}$  or equivalently  $\lambda_k \sim \frac{\Lambda}{\Delta_\lambda} = \frac{2}{N \Delta_\lambda}$  with  $k = 2 \dots, N_A$  with  $\Delta_\lambda$  as the mean level spacing of the Schmidt eigenvalues:  $\Delta_\lambda \sim 1/N$ . For  $\Lambda \ll \Delta_\lambda$ , this gives, from the definitions,  $R_0 \sim -N_A \log\left(\frac{\Lambda}{\Delta_\lambda}\right)$  and  $R_1 \sim \left(1 - \frac{\Lambda}{\Delta_\lambda}\right) \frac{\Lambda}{\Delta_\lambda} - \frac{N_A \Lambda}{\Delta_\lambda} \log\left(\frac{\Lambda}{\Delta_\lambda}\right)$ , thus implying  $R_0$  remaining very large and  $R_1$  negligible. A change however occurs  $\Lambda \sim \Delta_\lambda$  with  $R_0$  becoming finite and  $R_1$  large for  $\Lambda \gg \Delta_\lambda$ . This is also confirmed by our numerical analysis discussed in section VII.

Proceeding along the same route, we derive the  $\Lambda$  governed evolution of the variance of the von Neumann entropy, defined as  $\langle \delta R_1^2 \rangle = \langle R_1^2 \rangle - \langle R_1 \rangle^2$  (the details discussed in [11]).

$$\frac{\partial \langle \delta R_1^2 \rangle}{\partial \Lambda} = 2(Q - \langle R_1^2 \rangle) + N_B \text{cov}(R_0, R_1) - N \langle \delta R_1^2 \rangle \quad (41)$$

where  $Q \equiv \left\langle \sum_n \lambda_n (\log \lambda_n)^2 \right\rangle$  and  $\text{cov}(R_0, R_1)$  refers to the covariance of  $R_0$  and  $R_1$ :  $\text{cov}(R_0, R_1) \equiv \langle R_0 R_1 \rangle - \langle R_0 \rangle \langle R_1 \rangle$ . A general solution of eq.(41) for large  $N$ , arbitrary  $\Lambda$  and arbitrary initial conditions can now be given as

$$\langle \delta R_1^2 \rangle(\Lambda) \approx e^{-N\Lambda} \left( \langle \delta R_1^2 \rangle(0) + \int_0^\Lambda \left( 2(Q - \langle R_1^2 \rangle) + N_B \text{cov}(R_0, R_1) \right) e^{N\Lambda} d\Lambda \right) \quad (42)$$

In the large  $N$  limit and for small  $\Lambda$ , the term  $Q - \langle R_1^2 \rangle \ll \text{cov}(R_0, R_1)$  and the evolution of  $\langle \delta R_1^2 \rangle$  is dominated by the term  $\text{cov}(R_0, R_1)$ . Consequently, the above solution requires a prior knowledge of  $\Lambda$ -dependence of  $\text{cov}(R_0, R_1)$ . For initial state at  $\Lambda = 0$  chosen as separability limit,  $\langle \delta R_1^2 \rangle(0) = 0$ . A small change in  $\Lambda$  from 0 to, say  $\Lambda_1 \sim O(1/N)$  causes a rapid increases and thereafter decay of  $|\text{cov}(R_0, R_1)|$ ; eq.(42) then gives

$$\langle \delta R_1^2 \rangle(\Lambda) \approx c_0 N_B e^{-N(\Lambda - \Lambda_1)} \quad (43)$$

where  $c_0$  is the value of  $|\text{cov}(R_0, R_1)|$  at  $\Lambda = \Lambda_1$ . The above prediction is also confirmed by our numerics displayed in fig. 1. Indeed, we find the behavior of  $|\text{cov}(R_0, R_1)|$  qualitatively the same as  $\langle \delta R_1^2 \rangle$  (fig. 1), including their divergence.

In the large  $\Lambda$  limit, with  $R_0 \sim N_A R_1$ , the  $\text{cov}(R_0, R_1)$  almost vanishes and the term  $Q - \langle R_1^2 \rangle$  dominates, and eq.(42) now gives

$$\langle \delta R_1^2 \rangle(\Lambda) \approx 2 \frac{(Q - \langle R_1^2 \rangle)}{N} (1 - e^{-N\Lambda}) = 2 \frac{(Q - \langle R_1^2 \rangle)}{N} \frac{\langle R_1 \rangle(2\Lambda)}{\langle R_1 \rangle(\infty)} \quad (44)$$

In the ergodic limit  $\Lambda \rightarrow \infty$ ,  $Q - \langle R_1^2 \rangle \approx 1$ , then the above gives  $\langle \delta R_1^2 \rangle \sim \frac{2}{N}$  and is consistent with previous studies [2, 9, 24].

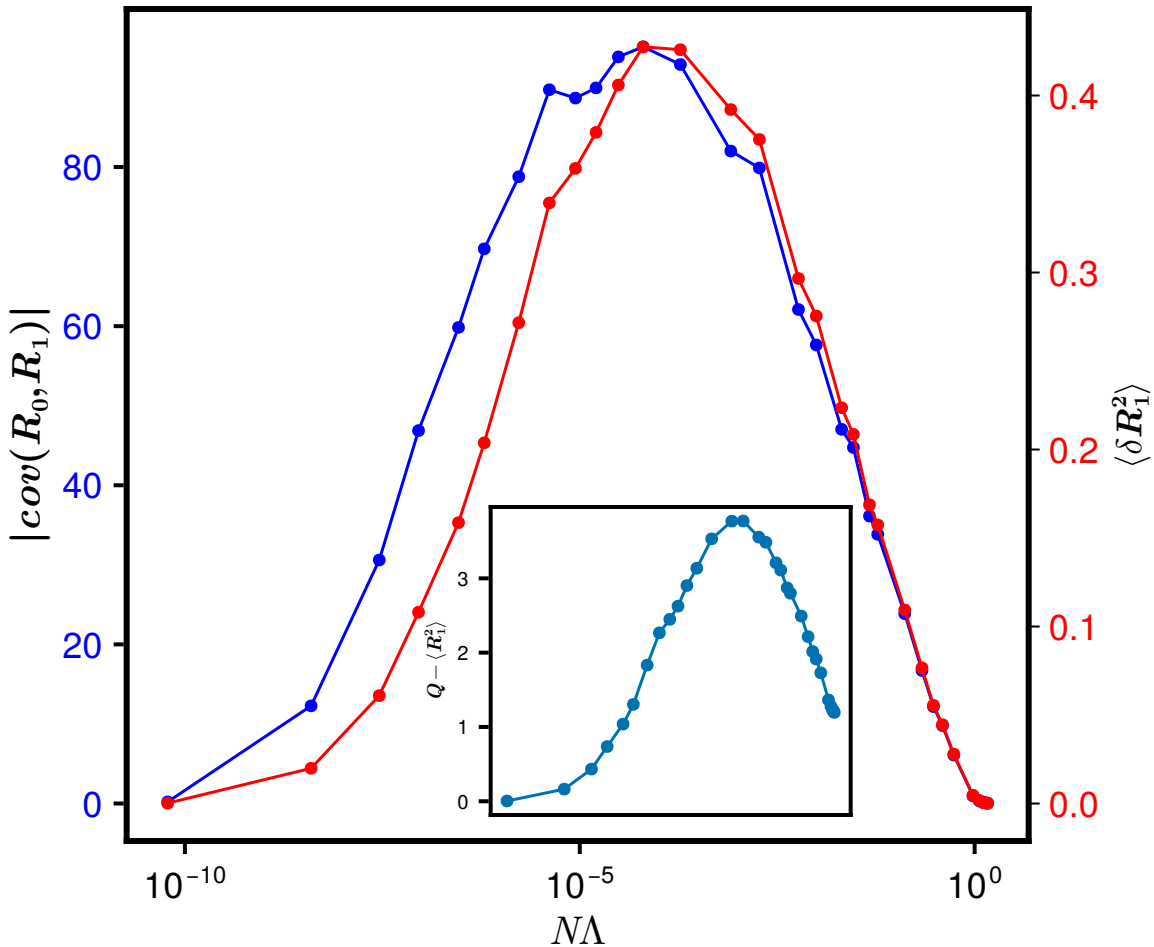


FIG. 1: **Analysis of the RHS of the eq. (41).** We compare the  $|\text{cov}(R_0, R_1)|$  (blue) and the  $\langle \delta R_1^2 \rangle$  (red) for the eigenstates of the QREM at  $E = 0$  for  $L = 14$ , and with the x-axis on a log scale. As can be seen, the quantities are qualitatively quite similar, and that in the ergodic regime the former tend to zero. The diverging variance of  $R_1$  is therefore a consequence of the diverging covariance  $\text{cov}(R_0, R_1)$ . (inset) We show the dynamics of  $Q - \langle R_1^2 \rangle$  (ref. eq. (41)), which is also diverging but  $\sim 1$  as  $\Lambda \rightarrow \infty$ , and hence dominates the covariance term in that limit. Similar results are obtained for the RFHM.

## VII. NUMERICAL ANALYSIS

A typical quantum state of a many-body Hamiltonian  $H$  depends in general on many system parameters governing its various physical attributes. For an ensemble density  $\rho(H)$  to be an appropriate representation of the statistical behaviour of  $H$ , the ensemble parameters must depend on the system parameters (as elucidated by the examples in section III). Thus,

a variation of any of the system parameters is expected in general to cause a variation of the ensemble parameters and thereby the entanglement statistics. Based on our theoretical prediction, however, the evolution of the entanglement statistics is governed only by two parameters, namely,  $\Lambda$  and  $N$  and not by the specific details of the ensembles parameters. Different states originating from similar initial conditions are then not only predicted to follow the similar paths in terms of  $\Lambda$ , they also correspond to same entanglement statistics if their  $\Lambda$ -values coincide. This indicates a potential classification of the quantum states of a given Hamiltonian (or different Hamiltonians subjected to same global symmetries and conservation laws) in non-ergodic universality classes characterized by the complexity parameter  $\Lambda$ . The ergodic universality class in this classification is characterized by  $\Lambda \rightarrow \infty$ . The deep significance of our theoretical claims makes it necessary to verify them numerically. For this purpose, we consider the Hamiltonian described by eq.(1) taken from the ensemble in eq.(3) and eq.(5) taken from the ensemble in eq.(6).

A physical Hamiltonian has in general many eigenstates characterized by their energies  $E$ . Consequently, an ensemble of Hamiltonians leads to many state ensembles, each representing a specific eigenstate and characterized by the state complexity parameter  $\Lambda = \Lambda(Y, E)$  where  $Y$  is the ensemble complexity parameter (alternatively stated, each point of the Hamiltonian spectrum corresponds to a state ensemble). An important point worth reemphasizing here is as follows. With  $\Lambda$ -dependent on energy range, the quantum states of the Hamiltonian  $H$  for different energies correspond in general to different  $\Lambda$  values, although each belongs to the same fixed set of system parameters, thus leading to same  $Y$ . If however the system parameters are varied, the entanglement measures for each state evolve through an analogous path lying between separability limit to maximum entanglement (their rates of evolutions however may vary).

The calculation of a measure, e.g.,  $R_1$  for an eigenstate say of energy  $E$  requires, in principle, an averaging over the corresponding state ensemble only. The numerical analysis however requires averaging over the neighbouring state ensembles too. This can be explained as follows. A state ensemble is obtained numerically by exactly diagonalizing an ensemble of Hamiltonians; the state ensemble  $P_c(C)$  then in principle corresponds to the set of eigenstates of energy  $E$  taken from each Hamiltonian of the ensemble  $\rho(H)$ . But as the spectrum locally fluctuates from one Hamiltonian to the other, it is not possible in general to pick the eigenstates with exactly same energy  $E$ . The state ensemble is then numerically obtained

by permitting a small fluctuation of energy, i.e., by considering the eigenstates within an energy range  $E \pm \delta E$  from each Hamiltonian. Here  $\delta E$  is an optimized range, permitting consideration of only those states in  $E \pm \delta E$  range which share same  $\Lambda$ . As the latter depends on  $R_{local}$ , the range  $\delta E$  should be chosen smaller than  $\Delta_{local} = (R_{local})^{-1}$  to ensure that  $\Lambda$  remains almost same for all the sample states in the ensemble.

For numerical determination of the eigenstates, we use the standard *shift-invert* diagonalization technique [25]. An efficient implementation of the technique and efficient computation for large systems leveraging MPI techniques is ensured by utilizing the SLEPc library in C [26] for our numerical codes. To quantify entanglement of an eigenstate, we consider the system represented by  $H$  divided into two halves, say  $A$  and  $B$  and calculate  $H$  matrix in their product basis. The information is further used to determine the von Neumann entropy ( $R_1 = -tr(\rho_A \log \rho_A)$ ) of the reduced state of one half of the system, i.e.,  $L_A = L/2$ , and throughout the subsequent analysis, we use log base 2 to calculate the entropy. The average of the measures are determined by both spectral and ensemble averaging. The specific details for each case are discussed below.

### A. QREM

In case of QREM, the Hamiltonian  $H$  has two system parameters, namely the transverse field strength  $\Gamma$ , which depends on  $b$ , and system size  $L$  and both appear in the ensemble density eq.(2) through ensemble parameters. Substitution of these values in eq.(19) leads to the complexity parameter  $Y - Y_0$  with the initial condition  $b = 0$

$$Y - Y_0 = -\frac{1}{2(N+1)\gamma} \sum_{r=0}^{L-1} \ln \left| 1 - \frac{2\gamma}{1 + (\frac{2^r}{b})^2} \right|. \quad (45)$$

The  $\sum_{r=0}^{L-1}$  above arises from the basis pairs  $|k\rangle$  and  $|l\rangle$  at a unit Hamming distance; the later correspond to the distance  $|k-l| = 2^r$  in the basis space, with  $r = 0 \dots L-1$ . Further, as  $\gamma$  is arbitrary (related to the variance of the matrix elements in the ergodic limit), we choose  $\gamma = 1/2$  in QREM numerical calculations.

We exactly diagonalize the Hamiltonian in eq. (1) for several values of the free parameter  $b$  ranging from 0, corresponding to a localized state, to a sufficiently large value such that the system reaches to the ergodic regime. Each  $b$  value for a fixed  $L$  however leads to many state ensembles characterized by  $\Lambda(e)$ ; the energy  $e$  can then be used as a free parameter

too. This in turn gives us a state ensemble with two free parameters  $b$  and  $e$  for a fixed  $L$ , and we can now seek whether the ensemble averaged measures, e.g.,  $\langle R_1 \rangle$  indeed coincides quantitatively for different pairs of  $b$  and  $e$  but same  $\Lambda$ .

As mentioned in the beginning of this section, it is necessary to consider the behaviour of entanglement measures subject to both ensemble and spectral averages. For this purpose, we consider the average of  $R_1$  and its variance over various disorder realizations and over about 1% of the total eigenstates per realization in the neighborhood of energy  $e = E$ , with corresponding  $\Lambda$ -values calculated from eq. (35). In earlier works on spectral statistics [27] and eigenfunction statistics in one-body systems [28], the approximation  $\xi^d = \langle I_2 \rangle^{-1}$ , where  $I_2$  is the inverse participation ratio (IPR) turned out to be consistent. However, in the present many-body case, this is not so. We find that in the present case, the average localization length ( $\xi^d$ ) is related to the covariance ( $\Omega_e$ )

$$\frac{\xi^d}{N} = \sum_{n=1}^{N_f-1} |\langle U(e_0 = E) | U(e_n) \rangle|^2 \equiv \Omega_e, \quad (46)$$

where,  $N_f$  is the number of eigenstates near the targeted energy  $E$  considered for ensemble averaging. The covariance  $\Omega_e$  varies between  $1/N$  and 1 corresponding to the localized and ergodic regimes respectively. The above relation, eq. (46), is motivated by the definition of  $R_{local}(E)$  given in Section V A, i.e.,  $\Omega_e$  is a measure of correlation of the eigenstate at energy  $E$  with the other eigenstates, and hence is useful in relating  $R_{local}(E)$  to the mean level density  $R(E)$ .

In contrast to spectral statistics characterized only by spectral complexity parameter  $\Lambda_e$ , the eigenvector statistics depend on both  $\Lambda$  and the system size. Furthermore, calculating  $\Lambda$  further requires knowledge about  $\chi_0$  which is determined numerically and is listed in the Table I for different cases.

Figs. 2 show the evolution of the average and the variance of the von Neumann entropy ( $R_1$ ) for a fixed system size,  $L = 14$ , but for different energies  $E$ . We average over 1000 disorder realizations and 200 eigenvectors per realization ( $N_f$ ) for various off-diagonal disorder parameter  $b$  and energy levels  $E$ . As shown in the Table I,  $\chi_0$  for different statistical measures turns out to be different. In fact, this was already predicted theoretically in Ref. [10], that  $\Lambda$  for different measures can indeed be different. Table I also shows the final form of  $\Lambda$  which is used in the figures. As is clear from the figures, that the evolution path of the entanglement statistics at different energy scales is indeed different (see inset), nevertheless,

with  $N\Lambda$  they show a universal evolutionary path and the different curves collapse onto each other. Also, note that the average  $R_1$  doesn't saturate to the same value in the ergodic limit. This behavior can also be succinctly explained in terms of  $\Lambda$ : At higher energy, the energy levels are far apart and the mean level density decreases sharply, resulting in a smaller  $\Lambda$  and hence lower entanglement.

In order to further justify the claim that the entanglement statistics at different energy levels should show similar behavior as long as  $N\Lambda$  remains same, in Fig. 3 we study the distribution of  $R_1$  in three different regimes, localized, non-ergodic and ergodic, characterized by fixing  $N\Lambda$  to small, intermediate, and large respectively; the latter also implies small, intermediate and large average entanglement respectively. As noted earlier, the  $\Lambda$  for different statistical measures turn out to be different, question arises which  $\Lambda$  to use for the distribution. From the Fig. 2 it is clear that the variance requires a rescaling by its maximum to observe the collapse and that the maximum variance is energy dependent; see Fig. 4. Consequently, to compare the distribution at different energy scales we use the  $\Lambda$  corresponding to the average  $R_1$ , such that the mean of the distribution across different parameters remain the same.

Fixing  $N\Lambda$  leads to a conspiracy between the parameters  $b$  and  $E$  to keep the  $N\Lambda$  same, and can be achieved in different ways as shown in the Table II. As is clear from Fig. 3, the distribution of  $R_1$  in the bulk of the energy spectrum deviates from that on the boundary. This can be attributed to the difference between the magnitude of the respective variances as

TABLE I:  $\chi_0$  and  $\Lambda$  for different models and measures. We display the numerically determined form of  $\chi_0$  and the  $\Lambda$  parameters for the QREM and the RFHM for the different statistical measures, viz., the average and the variance of the von Neumann entropy.

Model	Measure	$\chi_0$	$\Lambda$
QREM	$\langle R_1 \rangle$	$\frac{\Delta_e}{\langle I_2 \rangle}$	$\frac{-\frac{1}{2N\gamma} \sum_{r=0}^{L-1} \ln  1 - \frac{2\gamma}{1+(\frac{2r}{b})^2} }{\Delta_e} \frac{\Omega_e^2}{\langle I_2 \rangle}$
	$\langle \delta R_1^2 \rangle$	$(\Delta_e)^{-0.4}$	$\frac{-\frac{1}{2N\gamma} \sum_{r=0}^{L-1} \ln  1 - \frac{2\gamma}{1+(\frac{2r}{b})^2} }{(\Delta_e)^{2.4}} \Omega_e^2$
RFHM	$\langle R_1 \rangle$	$\Delta_e^{3.1} \Omega_e^{1.5}$	$\frac{1}{\gamma} \ln \left( \frac{h_0^4}{h^4} \frac{D}{D_0} \right) \Delta_e^{1.1} \Omega_e^{3.5}$
	$\langle \delta R_1^2 \rangle$		

shown in the Fig. 4; nevertheless, the distributions are qualitatively similar. Furthermore, a slight deviation in the distributions of the bulk states,  $E = 0$  and  $E = 5$ , and similarly for the edge states,  $E = 8$  and  $E = 9$ , is due to the slight difference in their  $\Lambda$  values (see  $(N\Lambda)_{calc}$  in the Table II).

## B. RFHM

Our numerical analysis in this case is based on the Hamiltonian  $H$  in eq.(5) with  $J = 1$ ,  $h_j$  as the Gaussian disorders with mean zero, and  $\rho(H)$  given by eq.(6). A substitution of

TABLE II: The table shows the system parameters,  $b$  and  $E$  for the QREM, and  $h$  and  $D$  for the RFHM, corresponding to a targeted  $N\Lambda$ , and the calculated value  $(N\Lambda)_{calc}$  with those parameters for the respective systems. These parameters are then used in studying the distribution of  $R_1$  in Figs. 3 and 8.

QREM				RFHM			
$N\Lambda$	$(N\Lambda)_{calc}$	$b$	$E$	$N\Lambda$	$(N\Lambda)_{calc}$	$h$	$D$
$10^{-6}$	$6.17 \times 10^{-7}$	5.0	0.0	$10^{-4}$	$9.92 \times 10^{-5}$	3.7	0.1
	$8.47 \times 10^{-7}$	15.0	5.0		$1.12 \times 10^{-4}$	4.1	0.5
	$9.25 \times 10^{-7}$	70.0	8.0		$1.03 \times 10^{-4}$	4.4	1.0
	$4.4 \times 10^{-7}$	101.0	9.0		$1.04 \times 10^{-4}$	4.7	1.5
						$1.23 \times 10^{-4}$	5.0
$10^{-3}$	$8.17 \times 10^{-4}$	30.0	0.0	$5 \times 10^{-2}$	$4.29 \times 10^{-2}$	1.5	0.1
	$1.25 \times 10^{-3}$	70.0	5.0		$6.44 \times 10^{-2}$	1.9	0.5
	$1.09 \times 10^{-3}$	501.0	8.0		$5.05 \times 10^{-2}$	2.2	1.0
	$9.47 \times 10^{-4}$	1500.0	9.0		$6.7 \times 10^{-2}$	2.4	1.5
					$6.8 \times 10^{-2}$	2.5	2.0
$10^{-1}$	$1.03 \times 10^{-1}$	115.0	0.0	20.0	21.2	0.4	0.1
	$9.5 \times 10^{-2}$	210.0	5.0		18.4	0.9	0.5
	$1.05 \times 10^{-1}$	2000.0	8.0		20.5	1.1	1.0
	$9.52 \times 10^{-2}$	70000.0	9.0		20.7	1.2	1.5
					23.0	1.2	2.0

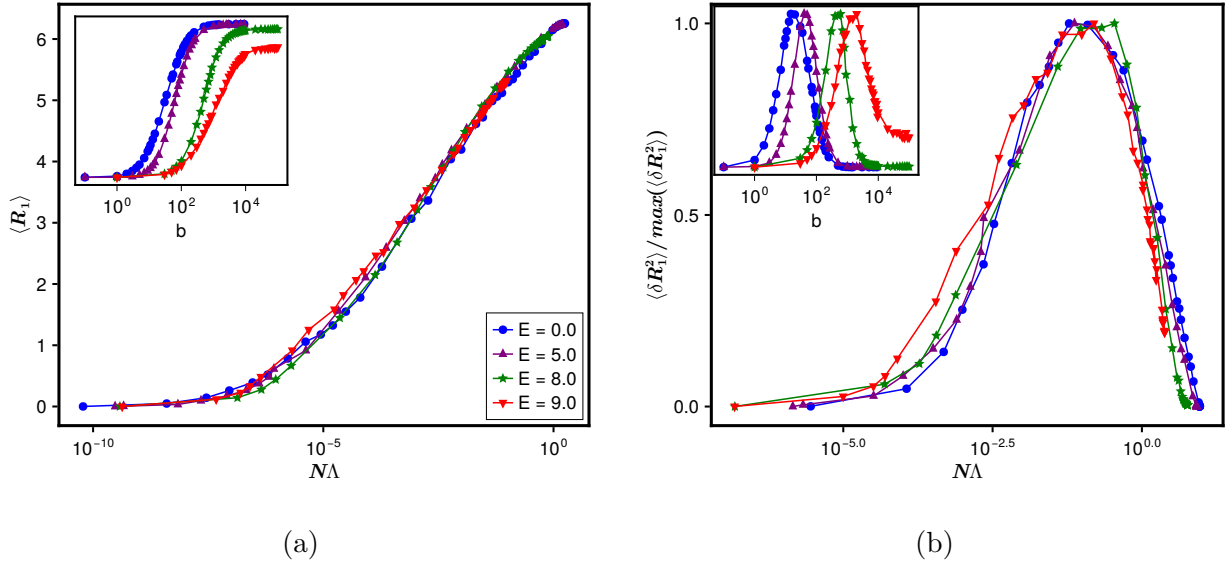


FIG. 2: **Average and variance of von Neumann Entropy in the QREM.** (a) The dynamics of the average and (b) the variance of the von Neumann entropy  $R_1$ , for the system size  $L = 14$  over 1000 disorder realizations, and 200 eigenstates per realizations at different energy scales ( $E$ ) is shown. The y-axes in (b) has been rescaled by the maximum for a better comparison, as the maximum variance is energy dependent (see Fig. 4). As can be seen, the evolution curves for different energies overlap when plotted with  $N\Lambda$ , as opposed to with the system parameter  $b$  (see inset). The  $\Lambda$  for the respective measures is shown in the Table I.

values given by eq.(9) in eq.(22) and further using eqs. (21), eq. (22) can be approximated in the large  $L$  limit to give (see [11] for details)

$$Y - Y_0 \approx \frac{1}{\gamma} \log \left( \frac{h_0^4 D}{h^4 D_0} \right), \quad (47)$$

where,  $h_0$  and  $D_0$  correspond to initial conditions  $h_0 \gg 1$  and  $D_0 = 1.0$ , and in the numerical calculations we take  $\gamma = 1$ .

As  $H$  in this case conserves the total spin in the z-direction ( $S_z^{total} = \sum_{i=1}^L S_i^z$ ), it is useful to consider  $S_z$  basis for its matrix representation. The choice leads to a block diagonal  $H$  matrix, with different blocks corresponding to different  $S_z^{total}$  values. For even  $L$ , we focus on the  $S_z^{total} = 0$  block, which is the largest block of dimension  $M = \frac{L!}{\frac{L}{2}! \frac{L}{2}!}$ . The diagonalization of the block leads to  $M$  non-zero components of an eigenstate  $\Psi$  of  $H$  with  $S_z^{total} = 0$ ; the rest of the components of  $\Psi$  are zero (due to  $H$  preserving  $S_z^{total}$ -symmetry). An efficient

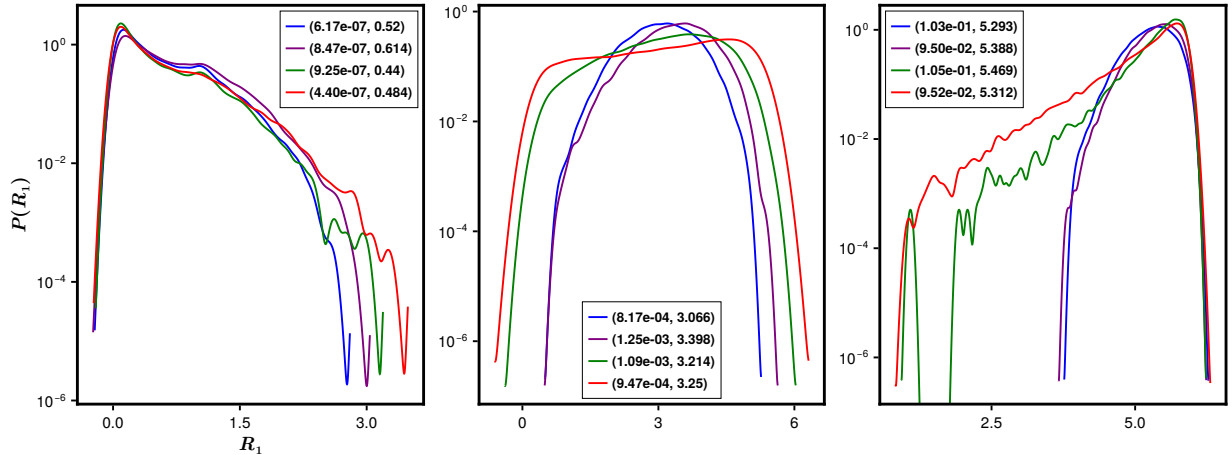


FIG. 3: **Distribution of von Neumann entropy in the QREM.** The distribution of  $R_1$  (on a log scale) in the localized, non-ergodic, and ergodic regimes is shown. The different regimes are solely characterized by fixing  $N\Lambda$ , letting the parameters  $b$  and the energy  $E$  vary; see Table II for details. The difference between the distributions for eigenstates at the boundary and bulk is due to the different in their variance (Fig. 4) although qualitatively they are the same.

method to calculate the von Neumann entropy for this case is described in Ref. [29]. With  $H$  as a real-symmetric matrix in the chosen basis, the components of its eigenstates are real variables as well.

We exactly diagonalize the Hamiltonian in eq. (5) for several system sizes with a fixed parameter  $D = 1.0$ , and for several values of the parameter  $D$  with a fixed system size  $L = 14$ . As in the case of QREM, here again we consider both spectral and ensemble averaging, however in this case we focus only on the bulk energy spectrum. For spectral averaging, we choose 100 eigenstates at  $E = 0$  (except for  $L = 12$  where we consider only 50 eigenpairs), and for the ensemble averaging, the size of the ensemble is chosen based on system size: for  $L = 12, 14, 16, 18$ , the chosen ensemble sizes are 2000, 1000, 500, 200 respectively. To proceed further, we also need to determine  $\Lambda$  defined in eq. (35). Besides  $Y - Y_0$ , this requires a prior knowledge of local mean level spacing  $\Delta_e$  as well as average localization length  $\xi$  as a function of  $h$ . In absence of a theoretical formulation, we determine  $\Delta_e$  numerically,  $\xi$  is again determined using the relation eq. (46), and  $\chi_0$  is shown in the Table I, which is also determined numerically. This, along with substitution of (47) in eq.

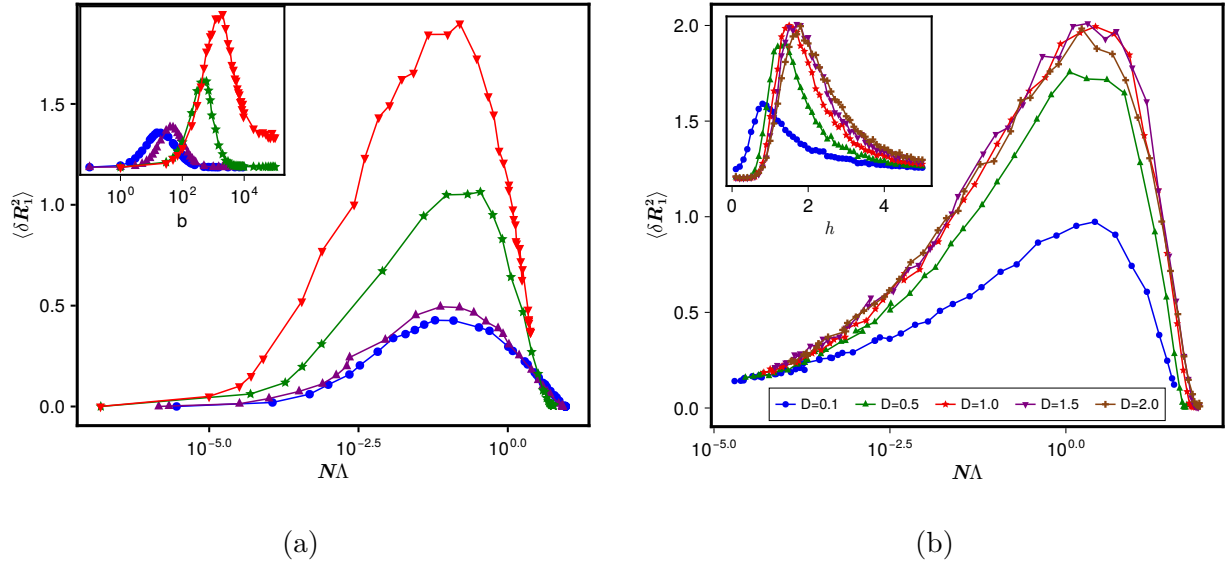


FIG. 4: **Variance of von Neumann entropy.** The figure displays the evolution of the von Neumann entropy variance ( $\langle\langle\delta R_1^2\rangle\rangle$ ) for (a) the QREM and (b) the RFHM. In contrast to Figs. 2(b) and 7(b), the y-axis in this case is not rescaled by their maximum. Clearly, the maximum variance for the higher energies in (a) and for smaller anisotropy parameter  $D$  in (b) is different from the other cases. Consequently, the corresponding distributions of  $R_1$  in Figs. 3 and 8, also show deviations; nevertheless, they agree qualitatively.

(35) then gives  $\Lambda$  for the  $H$  in eq. (5), and is shown in the Table I.

Figs. 5 display the behavior of average and variance of  $\langle R_1 \rangle$  with varying field strength  $h$  and system sizes  $L$  for a fixed  $D = 1.0$ . The y-axes of the figures are rescaled by their maximum to avoid finite-size effects. As noted earlier, the eigenfunction statistics depends on both the system size and  $\Lambda$ , as is clear from the figures, the evolution curves corresponding to different system sizes show a close collapse for large system sizes with  $N\Lambda$ , while their distinctive feature with the disorder parameter  $h$  is displayed in the inset for a comparison. Using  $N\Lambda$  as the governing parameter is, in fact, motivated from the evolution equations, eq. (39) and eq. (42). The inset in the Fig. 5(a) also reveals a crossing of the different curves for different system sizes and thus indicates a phase transition from the ergodic to many-body localized regimes. This invites us to question the role of  $\Lambda$  in characterizing phase transition in the system.

As mentioned above, the rescaled complexity parameter  $N\Lambda$  is in general a function of  $N$  and approaches, therefore, either 0 or  $\infty$  in the thermodynamic limit, thereby implying

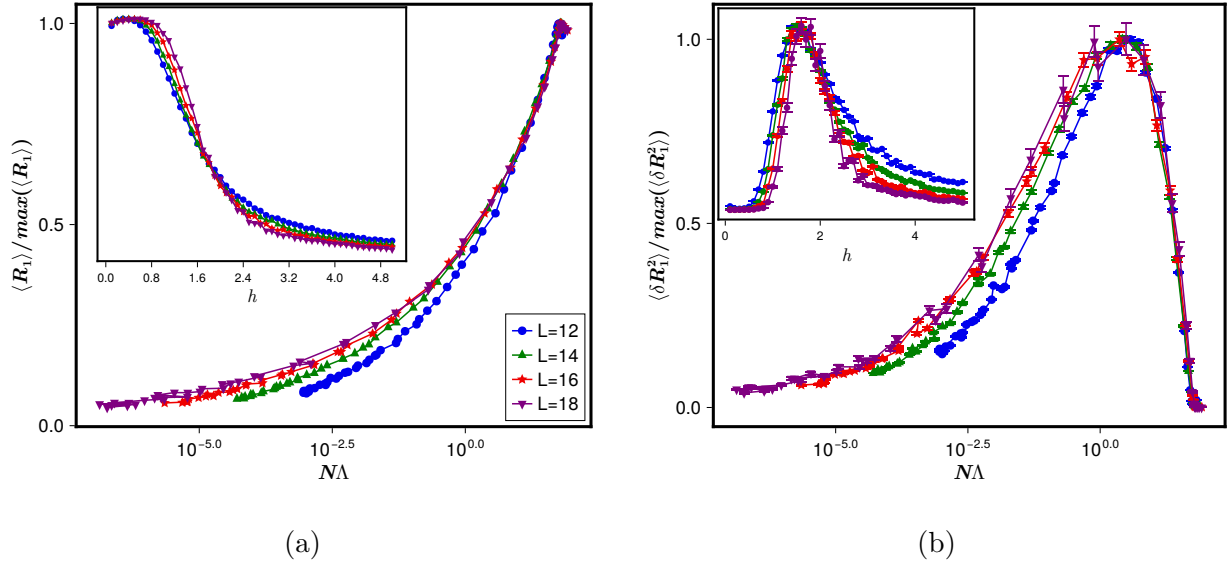


FIG. 5: **Average and variance of von Neumann entropy in the RFHM (varying  $L$ ).** (a) The dynamics of the average and (b) the variance of the von Neumann entropy over various disorder realizations, and 100 (50 for  $L = 12$ ) eigenstates per realizations for various system sizes, but fixed  $D = 1.0$ , is shown. The y-axes have been rescaled by their maximum value to avoid finite-size effects. As can be seen, the evolution curves for different system sizes overlap when plotted with  $N\Lambda$ , as opposed to with disorder strength  $h$  (see inset).

the localized or the ergodic regime of the eigenfunction dynamics respectively [10, 22]. A subtle conspiracy of the system conditions however may render  $N\Lambda$  independent of  $N$ ; the statistics under such conditions displays a critical behavior and remains different from both the localized or ergodic regimes even in limit  $N \rightarrow \infty$ . As shown in the Fig. 6, this behavior is indeed displayed for RFHM:  $N\Lambda$  for different system sizes with the disorder parameter  $h$  intersect each other and hence becomes size-independent at that point, while going to zero and  $\infty$  in the localized and the ergodic regimes respectively. A finite-size scaling analysis for  $N\Lambda$  is also shown in the inset. The critical point  $h_c$  and the critical exponent  $\nu$  is different from the values reported in the previous works and is due to the Gaussian randomness considered in this work as opposed to the uniform randomness considered there [16, 18]. Fig. 6 then suggests the following

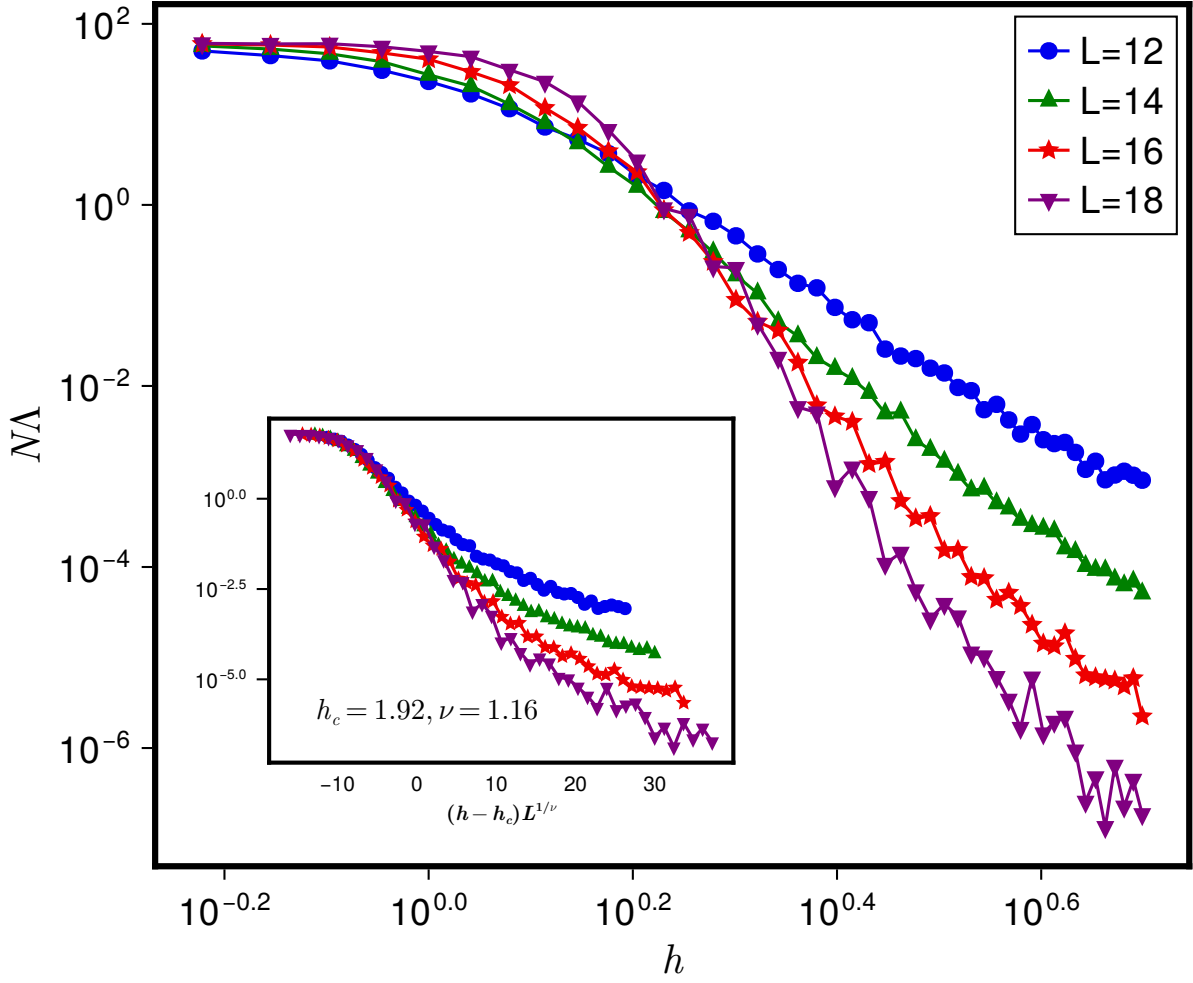


FIG. 6: **Finite-size scaling of  $N\Lambda$  in the RFHM.** The figure displays the dependence of parameter  $N\Lambda$  on the field strength  $h$  for various system sizes  $L$ . As clearly visible from the figure,  $N\Lambda$  becomes size independent at the critical point  $h_c$ . A finite-size scaling analysis with the critical point and exponent is also shown in the inset.

$$\frac{\langle R_1 \rangle}{\langle R_1 \rangle_{max}} = f(N\Lambda) = f((h - h_c)L^{1/\nu}). \quad (48)$$

To validate our theoretical claim regarding  $\Lambda$  as the single parameter that governs the localization-to-delocalization crossover if the system size is fixed, we study the evolution of entanglement for different anisotropy strength  $D$  but fixed system size  $L = 14$ . Figs. 7 show the evolution of the average and variance of  $R_1$  with  $\Lambda$  and with  $h$  in the inset. As is clear from the figures, the curves for different  $D$  indeed collapse onto each other with  $\Lambda$ ,

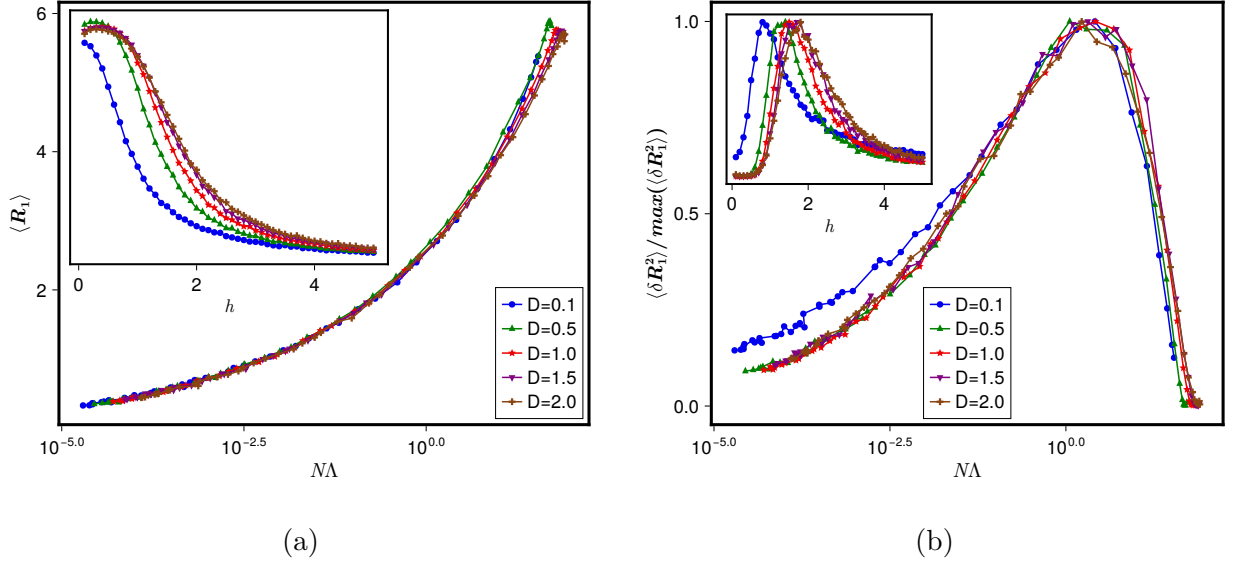


FIG. 7: **Average and variance of von Neumann Entropy in the RFHM (varying  $D$ ).** The details here are same as Fig. 5, however, in this case we study the dynamics for varying anisotropy parameter  $D$  while keeping the system size fixed,  $L = 14$ . In this case as well, the evolution curves for different  $D$  show a common path with  $N\Lambda$ .

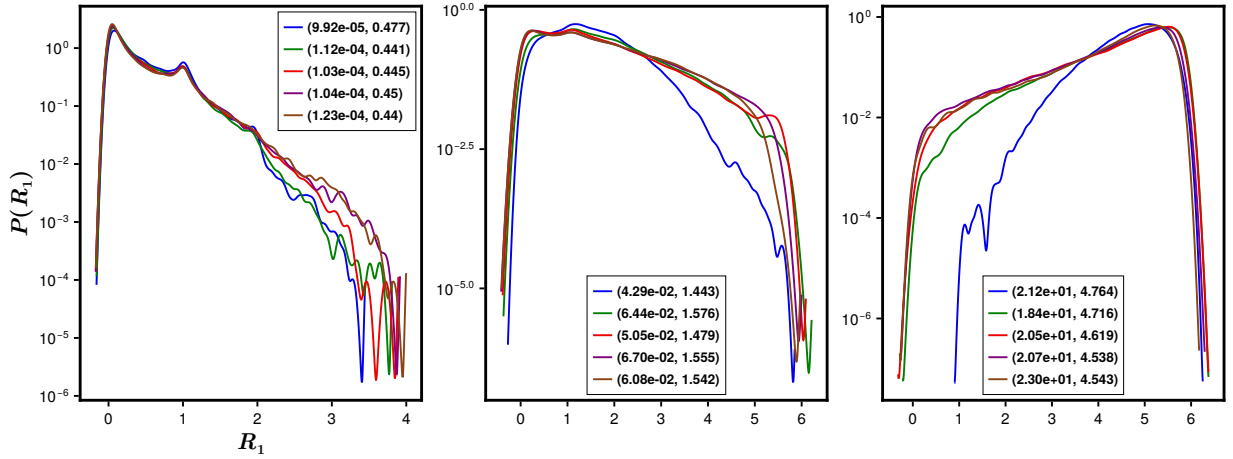


FIG. 8: **Distribution of von Neumann entropy in the RFHM.** The distribution of  $R_1$  in localized, non-ergodic, and ergodic regimes is shown. The different regimes are solely characterized by fixing  $N\Lambda$ , letting the parameters  $h$  and  $D$  vary; see Table II for details. We find that the distributions show a close collapse, except for the case  $D = 0.1$  which is because the variance of  $R_1$  for  $D = 0.1$  is much smaller than compared to other cases (see Fig. 4).

although they show a distinctive evolution with  $h$ . Furthermore, in the Fig. 8, we also study the distribution of  $R_1$  in the localized, critical, and ergodic regimes, characterized by small, intermediate, and large  $N\Lambda$  respectively similar to the Fig. 3 for the QREM. In this case, fixing  $N\Lambda$  leads to different combinations of  $h$  and  $D$  as shown in the Table II. Also, as shown in the Fig. 4(b), the maximum variance of  $R_1$  is weakly dependent on  $D$  except for small values of  $D$ . This also leads to the slightly deviating distribution of  $R_1$  for  $D = 0.1$ .

As indicated by many previous studies, increase in  $h$  also causes a crossover of the quantum dynamics of  $H$  from a localized to ergodic regime. This hints at an underlying connection between the two type of quantum correlations involved in the separable to entangled state transition and those in the localization to ergodic state transition. In general, the two type of quantum correlations are of different type, the former measured by various entanglement measures and the latter by average localization length, or inverse participation ratio etc. In addition, contrary to the entanglement analysis requiring at least a bipartite basis, the localization analysis can occur in a monopartite basis. But, in the present case, both transitions are analyzed in same basis i.e. configuration basis, a correspondence between two types is indeed expected.

## VIII. CONCLUSION

In the end we summarize our main ideas, results and open questions. As complicated interactions / disorder usually render an exact determination of a many-body Hamiltonian matrix in any physically motivated basis a mathematically intractable task, consideration of their representation by an ensemble is in general unavoidable. In this work, we have theoretical analyzed the entanglement dynamics, as the system conditions vary, of the eigenstates of the many-body Hamiltonians which can be well-represented by the multiparametric Gaussian ensembles of Hermitian matrices in a bipartite basis (with uncorrelated / pairwise correlated matrix elements and symmetry resolved to ensure nondegeneracy of the eigenstates). As shown in a series of previous studies, the dynamics of Hamiltonian ensemble in the matrix space is governed by a single functional  $Y$  of all system conditions, referred to as ensemble complexity parameter. The Hamiltonian ensemble in turn gives rise to an infinite range of state ensembles, each characterized by the state complexity parameter  $\Lambda$  which depend on energy of the state as well as  $Y$  (and thereby system condition). Our analysis indicates

the existence of a common evolutionary path of the entanglement measures governed by  $\Lambda$ . With the system dependence appearing collectively through  $\Lambda$ , a knowledge of the latter is sufficient to track the effect of varying system conditions on the entanglement measures of a given state. This indicates a potential application of the  $\Lambda$ -formulation in achieving the holy grail of the quantum state engineering: the approach to Haar-state starting from an arbitrary quantum state of a many-body Hamiltonian through a controlled variation of the system conditions.

Besides Hamiltonian parameters,  $\Lambda$  depends on the energy of the eigenstates too and can in general vary for different eigenstates of a given Hamiltonian notwithstanding same set of system conditions. Under a variation of the system conditions however, the entanglement statistics for all eigenstates evolve along a common path lying between separability and maximum entanglement limit. The complexity parameter formulation can thus be used to compare the relative entanglement characteristics of different eigenstates of a give Hamiltonian under a fixed set of system conditions and can thereby act as a distance measure between two states. The above statements are however applicable only if the changing system conditions do not change the global constraints class of the Hamiltonian ensemble: as the path depends on the global constraints of the Hamiltonian and thereby on the complexity path constants of the ensemble, it need not remain same if the system conditions affect the global constraints too, e.g., breaking the symmetry conditions, conservation laws too.

We emphasize that most of the theoretical results in our analysis are derived through exact routes and without approximations. The importance of our results nonetheless rendered it highly desirable to seek their numerical validation. This however required exact diagonalization of large sized ensembles on many-body systems, confined not only to a single set of system conditions but also for many such sets to verify the existence of a common complexity path. A numerical determination of  $\Lambda$  is also a challenging task. While we have achieved the verification based on the numerical analysis of two standard many-body system, namely the quantum random energy model and the random field Heisenberg model, a thorough numerical analysis by research groups better numerically equipped is very desirable.

## IX. ACKNOWLEDGMENT

We thank Dr. Ivan Khaymovich, Nordita for the suggestion to consider random field ising model for our numerical analysis. We acknowledge National Super computing Mission (NSM) for providing computing resources of ‘PARAM Shakti’ at the IIT Kharagpur, which is implemented by C-DAC and supported by the Ministry of Electronics and Information Technology (MeitY) and Department of Science and Technology (DST), Government of India. One of the authors (P.S.) is also grateful to SERB, DST, India for the financial support provided for the research under Matrics grant scheme. D.S. acknowledges financial support from the MHRD through the PMRF scheme.

- 
- [1] K. Życzkowski, K. A. Penson, I. Nechita, and B. Collins, “Generating random density matrices,” *Journal of Mathematical Physics*, vol. 52, no. 6, 2011.
  - [2] C. Nadal, S. N. Majumdar, and M. Vergassola, “Statistical distribution of quantum entanglement for a random bipartite state,” *Journal of Statistical Physics*, vol. 142, pp. 403–438, 2011.
  - [3] S. Kumar and A. Pandey, “Entanglement in random pure states: spectral density and average von neumann entropy,” *Journal of Physics A: Mathematical and Theoretical*, vol. 44, no. 44, p. 445301, 2011.
  - [4] S. N. Majumdar, “Extreme eigenvalues of wishart matrices: application to entangled bipartite system,” *arXiv preprint arXiv:1005.4515*, 2010.
  - [5] B. Collins and I. Nechita, “Random matrix techniques in quantum information theory,” *Journal of Mathematical Physics*, vol. 57, 1 2016.
  - [6] I. Bengtsson and K. Życzkowski, *Geometry of quantum states: an introduction to quantum entanglement*. Cambridge university press, 2017.
  - [7] D. Shekhar and P. Shukla, “Entanglement dynamics of multi-parametric random states: a single parametric formulation,” *Journal of Physics A: Mathematical and Theoretical*, vol. 56, p. 265303, jun 2023.
  - [8] D. Shekhar and P. Shukla, “Edge of entanglement in nonergodic states: A complexity parameter formulation,” *Phys. Rev. E*, vol. 112, p. 024122, Aug 2025.

- [9] D. Shekhar and P. Shukla, “Distribution of the entanglement entropies of nonergodic quantum states,” *Phys. Rev. E*, vol. 112, p. 024123, Aug 2025.
- [10] P. Shukla, “Eigenfunction statistics of complex systems: A common mathematical formulation,” *Physical Review E - Statistical, Nonlinear, and Soft Matter Physics*, vol. 75, 5 2007.
- [11] D. Shekhar and P. Shukla, “supplementary material,”
- [12] C. R. Laumann, A. Pal, and A. Scardicchio, “Many-body mobility edge in a mean-field quantum spin glass,” *Physical Review Letters*, vol. 113, 11 2014.
- [13] C. L. Baldwin, C. R. Laumann, A. Pal, and A. Scardicchio, “The many-body localized phase of the quantum random energy model,” *Physical Review B*, vol. 93, 1 2016.
- [14] G. Biroli, D. Facoetti, M. Schiró, M. Tarzia, and P. Vivo, “Out-of-equilibrium phase diagram of the quantum random energy model,” *Physical Review B*, vol. 103, 1 2021.
- [15] T. Parolini and G. Mossi, “Multifractal dynamics of the qrem,” 7 2020.
- [16] D. J. Luitz, N. Laflorencie, and F. Alet, “Many-body localization edge in the random-field heisenberg chain,” *Physical Review B*, vol. 91, no. 8, p. 081103, 2015.
- [17] D. J. Luitz, “Long tail distributions near the many-body localization transition,” *Phys. Rev. B*, vol. 93, p. 134201, Apr 2016.
- [18] W. Buijsman, V. Cheianov, and V. Gritsev, “Random matrix ensemble for the level statistics of many-body localization,” *Physical review letters*, vol. 122, no. 18, p. 180601, 2019.
- [19] P. Shukla, “Random matrices with correlated elements: A model for disorder with interactions,” *Phys. Rev. E*, vol. 71, p. 026226, Feb 2005.
- [20] P. Shukla, “Alternative technique for complex spectra analysis,” *Phys. Rev. E*, vol. 62, pp. 2098–2113, Aug 2000.
- [21] P. Shukla, “Disorder perturbed flat bands: Level density and inverse participation ratio,” *Physical Review B*, vol. 98, 8 2018.
- [22] P. Shukla, “Level statistics of anderson model of disordered systems: Connection to brownian ensembles,” *Journal of Physics Condensed Matter*, vol. 17, pp. 1653–1677, 3 2005.
- [23] D. N. Page, “Average entropy of a subsystem,” *Physical review letters*, vol. 71, no. 9, p. 1291, 1993.
- [24] E. Bianchi and P. Dona, “Typical entanglement entropy in the presence of a center: Page curve and its variance,” *Physical Review D*, vol. 100, no. 10, p. 105010, 2019.

- [25] F. Pietracaprina, N. Macé, D. J. Luitz, and F. Alet, “Shift-invert diagonalization of large many-body localizing spin chains,” *SciPost Physics*, vol. 5, no. 5, p. 045, 2018.
- [26] V. Hernandez, J. E. Roman, and V. Vidal, “SLEPc: A scalable and flexible toolkit for the solution of eigenvalue problems,” *ACM Trans. Math. Software*, vol. 31, no. 3, pp. 351–362, 2005.
- [27] T. Mondal and P. Shukla, “Spectral statistics of multiparametric gaussian ensembles with chiral symmetry,” *Physical Review E*, vol. 102, 9 2020.
- [28] D. Shekhar and P. Shukla, “Single-particle entanglement dynamics in complex systems,” *Entropy*, vol. 28, no. 1, p. 29, 2025.
- [29] T. Zhou and D. J. Luitz, “Operator entanglement entropy of the time evolution operator in chaotic systems,” *Physical Review B*, vol. 95, no. 9, p. 094206, 2017.